Spectrochimica Acta Part A: Molecular and Biomolecular Spectroscopy 115 (2013) 154–174

Contents lists available at SciVerse ScienceDirect

Spectrochimica Acta Part A: Molecular and Biomolecular Spectroscopy

journal homepage: www.elsevier.com/locate/saa

Vibrational, NMR and quantum chemical investigations of acetoacetanilde, 2-chloroacetoacetanilide and 2-methylacetoacetanilide

V. Arjunan [a,*], M. Kalaivani [a], S. Senthilkumari [a], S. Mohan [b]

[a] Department of Chemistry, Kanchi Mamunivar Centre for Post-Graduate Studies, Puducherry 605 008, India
[b] School of Sciences and Humanities, VelTech University, Avadi, Chennai 600 062, India

HIGHLIGHTS

- Spectral analysis of acetoacetanilide and its derivatives were reported.
- The n(N11) → π*(C13=O14) interaction has strong stabilisation.
- Blue shift (45–50 cm^{-1}) in amide-II band of 2MAAA is observed than AAA.
- The amide-III modes are not affected by methyl and chloro substitution.
- A blue shift of amide-VI modes of 2MAAA and 2CAAA than AAA is observed.

GRAPHICAL ABSTRACT

The FTIR and FT-Raman spectra of acetoacetanilide (AAA), 2-chloroacetoacetanilide (2CAAA) and 2-methylacetoacetanilide (2MAAA) have been analysed. Quantum chemical studies were performed with B3LYP method using 6-311++G** and cc-pVTZ basis sets. The structural parameters, energies, thermodynamic parameters, vibrational frequencies and the NBO charges were determined. The ^{1}H and ^{13}C isotropic chemical shifts (δ ppm) with respect to TMS were also calculated using the gauge independent atomic orbital method. The delocaliation energy of the different types of bonding interactions was investigated. The influences of chloro and methyl groups on the characteristic frequencies of amide (—CONH—) have been discussed.

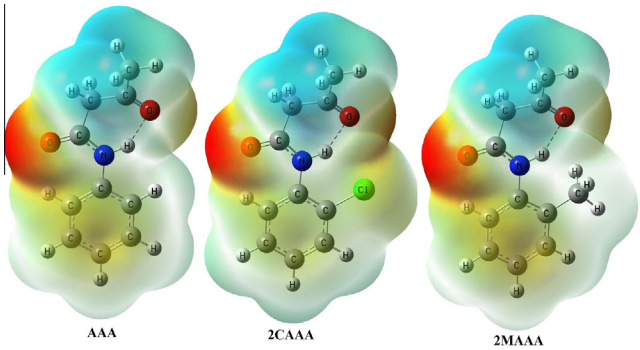

ARTICLE INFO

Article history:
Received 11 April 2013
Received in revised form 27 May 2013
Accepted 4 June 2013
Available online 20 June 2013

Keywords:
Acetoacetanilide
2-Chloroacetoacetanilide
2-Methylacetoacetanilide
DFT
FTIR
NMR

ABSTRACT

The vibrational assignment and analysis of the fundamental modes of the compounds acetoacetanilide (AAA), 2-chloroacetoacetanilide (2CAAA) and 2-methylacetoacetanilide (2MAAA) have been performed. Density functional theory studies have been carried out with B3LYP method utilising 6-311++G** and cc-pVTZ basis sets to determine structural, thermodynamic and vibrational characteristics of the compounds and also to understand the influence of chloro and methyl groups on the characteristic frequencies of amide (—CONH—) group. Intramolecular hydrogen bond exists in acetoacetanilide and *o*-substituted acetoacetanilide molecules and the N···O distance is found to be around 2.7 Å. The ^{1}H and ^{13}C nuclear magnetic resonance chemical shifts of the molecules were determined and the same have been calculated using the gauge independent atomic orbital (GIAO) method. The energies of the frontier molecular orbitals have been determined. In AAA, 2CAAA and 2MAAA molecules, the $n_N \rightarrow \pi^*_{CO}$ interaction between the nitrogen lone pair and the amide C=O antibonding orbital gives strong stabilization of 64.75, 62.84 and 64.18 kJ mol^{-1}, respectively. The blue shift in amide-II band of 2MAAA is observed by 45–50 cm^{-1} than that of AAA. The steric effect of ortho methyl group significantly operating on the

* Corresponding author. Tel.: +91 413 2211111, mobile: +91 9442635795; fax: +91 413 2251613.
E-mail address: varjunftir@yahoo.com (V. Arjunan).

http://dx.doi.org/10.1016/j.saa.2013.06.003

N—H bond properties. The amide-III, the C—N stretching mode of methyl and chloro substituted acetoacetanilide compounds are not affected by the substitution while the amide-V band, the N—H out of plane bending mode of 2-chloroacetoacetanilide compound is shifted to a higher frequency than that of AAA. The substituent chlorine plays significantly and the blue shift in *o*-substituted compounds than the parent in the amide-V vibration is observed. The amide-VI, C=O out of plane bending modes of 2MAAA and 2CAAA are significantly raised than that of AAA. A blue shift of amide-VI, C=O out of plane bending modes of 2MAAA and 2CAAA than AAA is observed.

Introduction

Acetoacetanilide and its derivatives are used in manufacturing agricultural chemicals, coating materials, dyes and pigments (the dry colours generally referred to as Hansa and benzidine yellows) as well as co-promoters for unsaturated polyesters. It is used in the productions of pyrazolone, light yellow 5G, acid complex yellow GR, neutral dark yellow GL, hansa yellow G and pigment yellow G. It is used as the raw materials in agriculture products of carboxin in pesticides, also can be used in medicine and organic synthesis. Diketene derivatives of acetoacetic acid and heterocycles have versatile applications including making agrochemicals, dyes, pigments, pharmaceuticals and stabilisers for PVC and polyester. Acetoacetanilide was known as chelating agent, and was used for determination of Fe(III) by spectrophotometric methods. Diazotisation of AAA leads to useful chelating agent.

Metazachlor is an acetoacetanilide herbicide used to control broad leaved weeds and annual grasses. It can also be used on ornamentals, nursery stock, in forestry and on wood land. It can control gramineous weeds and dicotyledonous weeds in the cole, soyabean, potato and tobacco fields. 2-Chloroacetoacetanilide and 2-methylacetoacetanilide are used as intermediate for the synthesis of organic pigments, pharmaceuticals and agrochemicals. The γ-chloroacetoacetanilide is used as spectrophotometric indicator for the EDTA titration of Fe (III) [1]. Bis-acetoacetanilide azo yellow and orange pigments, dyes, and dyestuffs are well known and are commonly used in various types of printing inks. They also generally provide effective colouration to certain substrates, such as plastics, paints, textiles, and the like. For example, Pigment Yellow 17 is a strong greenish-shade bis-acetoacetanilide yellow and has often been incorporated within plastics. Diazo pigments obtained from 3,3'-dichlorobenzidine and various acetoacetanilide compounds, which do not contain any water-soluble groups, have been used widely for the colouration of polyvinyl chloride resins, printing inks, paints and rubber. Acetoacetanilideisonicotinylhydrazone and its metal chelate exhibit anticancer activity. The studies on N-methylacetoacetanilideisonicotinylhydrazone and its metal chelates revealed that they were active against pathogenic fungal strains.

Recent studies suggest that organic materials have drawn substantial interest as potential candidates for applications in electro-optic and photonic devices, such as digital optical switches, light modulators, logic gates and high density optical data storage devices [2,3]. Extensive experimental and theoretical investigations of conjugated organic materials exhibiting large optical nonlinearities have been reported [4,5].

NLO organic materials are gaining widespread recognition and are under intensive investigation owing to their potential applications in the field of optical signal processing [6,7]. To possess NLO properties, organic molecules should contain a polar and highly conjugated *p*-electron system terminated with electron donor and acceptor groups. Acetoacetanilide and its derivatives having considerable interest, not least for their NLO properties, which make these compounds highly attractive for applications in frequency doubling of the light produced by semiconductor lasers [8,9].

Vijayan et al. [10] reported the growth and characterisation of nonlinear optical (NLO) single crystal acetoacetanilide. Ravikumar et al. [11] reported the vibrational contributions to the second-order nonlinear optical properties of *p*-conjugated structure acetoacetanilide. But the structural, vibrational and ^{1}H and ^{13}C chemical shifts of acetoacetanilide (AAA), 2-chloroacetoacetanilide (2CAAA) and 2-methylacetoacetanilide (2MAAA) have not been investigated. Thus, considering the industrial and biological importance of these compounds, extensive spectroscopic and theoretical quantum chemical studies were carried out on AAA, 2CAAA and 2MAAA and to understand the effect of methyl and chloro group on the characteristic frequencies of amide group.

Experimental

The compounds acetoacetanilide, 2-chloroacetoacetanilide and 2-methylacetoacetanilide were prepared from the respective aniline, 2-chloroaniline, 2-methylaniline and *t*-butylacetoacetate with dry xylene as solvent using the reported procedure [12].

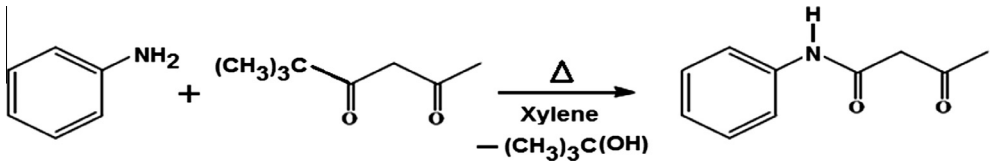

Scheme 1.

Table 1
Melting point and elemental analysis of the compounds.

Name of the compound	Melting point (°C)	% Found/(calculated)		
		C	H	N
Acetoacetanilide	83	67.72 (67.78)	6.19 (6.26)	7.87 (7.91)
2-Chloroacetoacetanilide	107	56.69 (56.75)	5.19 (5.24)	6.55 (6.62)
2-Methylacetoacetanilide	106	68.99 (69.08)	6.81 (6.85)	7.25 (7.32)

The reaction is represented by the Scheme 1. The pure samples of aniline, 2-chloroaniline, 2-methylaniline, *t*-butylacetoacetate and dry xylene were purchased from Aldrich chemicals, U.S.A and are used as such without further purification. All other chemicals used are of analar (AR) grade.

0.1 mol each of dry aniline (9.31 g), 2-chloroaniline (12.76 g) and 2-methylaniline (10.72 g), respectively is mixed with 15.82 g (0.1 mol) of *t*-butyl acetoacetate in 25 ml of pure dry xylene. The reaction mixture is then heated at 120 °C on a hot plate for about 15 min. The reaction was ceased after the evolution of *t*-butyl alcohol. The reaction mixture is allowed to cool; the crude solid products separate out. The synthesised crude compounds were recrystallised from acetone several times. The total yield of products acetoacetanilide; pale yellow needle like crystalline powder; m.p. 83–85 °C, 2-chloroacetoacetanilide; white or off-white powder; m.p. 107 °C and 2-methylacetoacetanilide; white or off-white powder; m.p. 104–106 °C is around 85%. The melting points were uncorrected. The purity of the compounds was confirmed by chemical analysis for C, H and N. The compounds prepared, the melting point and elemental analysis are presented in Table 1. The FTIR spectra of the compounds were recorded in the solid phase by KBr disc method in a Bruker IFS66 V spectrometer in the range 4000–400 cm^{-1}. The spectral resolution was 2 cm^{-1}. The FT-Raman spectra of these compounds were also recorded in the range 4000–400 cm^{-1} with the same instrument with FRA106 Raman modules. The light scattering was excited using a low-noise diode pumped Nd:YAG laser source operating at 1.064 μm with 200 mW power. A special (enhanced) liquid nitrogen cooled TGS detector was used. The frequencies of all sharp bands are accurate to 2 cm^{-1}. The ^1H (400 MHz; $CDCl_3$) and ^{13}C (100 MHz; $CDCl_3$) nuclear magnetic resonance (NMR) spectra were recorded on a Bruker HC400 instrument. Chemical shifts for protons are reported in parts per million scales (δ scale) downfield from tetramethylsilane.

Computational details

Since the amide group is highly polarisable, the DFT study is essential for the purpose of getting the structural parameters in precision with the standard high level 6-311++G** and the triple-ζ cc-pVTZ basis sets. Thus, the gradient corrected density functional theory (DFT) [13] with the three-parameter hybrid functional Becke3 (B3) [14,15] for the exchange part and the Lee–Yang–Parr (LYP) correlation functional [16], calculations have been carried out in the present investigation with Gaussian-09 [17] program. The harmonic vibrational frequency calculations were carried out resulting in IR and Raman frequencies together with intensities and Raman depolarisation ratios.

The molecular electrostatic potential (MEP) serves as a useful quantity to explain hydrogen bonding, reactivity and structure–activity relationship of molecules including biomolecules and drugs [18]. Isoelectronic molecular electrostatic potential surfaces (MEP) and electron density surfaces [19] were calculated using 6-311++G** basis set. The molecular electrostatic potential (MEP) at a point '*r*' in the space around a molecule (in atomic units) can be expressed as:

$$V(r) = \sum_A \frac{Z_A}{|\overrightarrow{R_A} - \vec{r}|} - \int \frac{\rho(\vec{r'})dr'}{|\vec{r'} - \vec{r}|}$$

where Z_A is the charge on nucleus A, located at R_A and $\rho(r')$ is the electronic density function for the molecule. The first and second terms represent the contributions to the potential due to nuclei and electrons, respectively. $V(r)$ is the resultant at each point r, which is the net electrostatic effect produced at the point r by both the electrons and nuclei of the molecule. GaussView 5.0.8 visualisation program [20] has been utilised to construct the MEP surface and the shape of frontier molecular orbitals.

The B3LYP method allows calculating the shielding constants with accuracy. The ^1H and ^{13}C NMR isotropic shielding were calculated using the GIAO method [21,22] using the optimised parameters obtained from B3LYP/6-311++G** method. The effect of $CDCl_3$ solvent on the theoretical NMR parameters was included using the PCM model. The isotropic shielding constant values were used to calculate the isotropic chemical shifts δ with respect to tetramethylsilane (TMS). The chemical shifts were determined by the relation $\delta_{iso}(X) = \sigma_{iso}(X)_{TMS} - \sigma_{iso}(X)$, where δ_{iso} – isotropic chemical shift and σ_{iso} – isotropic shielding constant.

The Raman scattering activities (S_i) calculated by Gaussian 09W program were suitably converted to relative Raman intensities (I_i)

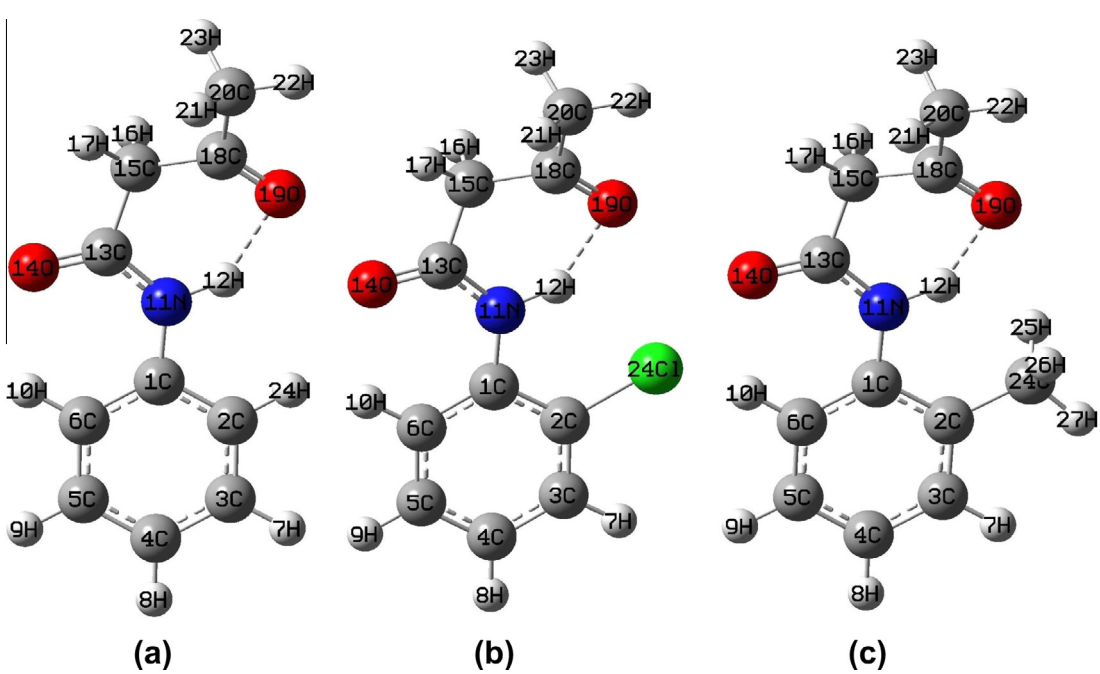

Fig. 1. The stable geometry and atom numbering of (a) acetoacetanilide and (b) 2-chloro acetoacetanilide and (c) 2-methylacetoacetanilide.

Table 2
Structural parameters calculated for acetoacetanilide (AAA), 2-chloroacetoacetanilide (2CAAA) and 2-methylacetoacetanilide (2MAAA) employing B3LYP methods with 6-311++G** and cc-pVTZ basic sets.

Structural parameters	AAA		2CAAA		Expt.[a]	2MAAA		Expt.[b]
	B3LYP/6-311++G**	B3LYP/cc-pVTZ	B3LYP/6-311++G**	B3LYP/cc-pVTZ		B3LYP/6-311++G**	B3LYP/cc-pVTZ	
Internuclear distance (Å)								
C1—C2	1.40	1.40	1.41	1.40	1.40	1.41	1.41	1.41
C1—C6	1.40	1.40	1.40	1.40	1.40	1.40	1.40	1.40
C1—N11	1.41	1.41	1.41	1.40	1.40	1.42	1.41	1.41
C2—C3	1.39	1.39	1.39	1.39	1.37	1.40	1.39	1.40
C2—H24	1.09	1.08						
C2—Cl24			1.76	1.76				
C2—C24						1.51	1.51	1.50
C3—C4	1.39	1.39	1.39	1.39	1.39	1.39	1.39	1.40
C3—H7	1.08	1.08	1.08	1.08	0.95	1.09	1.08	
C4—C5	1.39	1.39	1.39	1.39	1.39	1.39	1.39	1.38
C4—H8	1.08	1.08	1.08	1.08	0.95	1.08	1.08	
C5—C6	1.39	1.39	1.39	1.39	1.39	1.39	1.39	1.38
C5—H9	1.08	1.08	1.08	1.08		1.08	1.08	
C6—H10	1.08	1.08	1.08	1.08	0.95	1.08	1.08	
N11—H12	1.02	1.01	1.02	1.02	0.88	1.02	1.01	
N11—C13	1.36	1.36	1.37	1.36	1.36	1.36	1.36	1.36
H12—O19	1.95	1.94	1.98	1.98		1.97	1.96	
C13—O14	1.22	1.22	1.22	1.22	1.22	1.22	1.22	1.23
C13—C15	1.54	1.54	1.54	1.54	1.52	1.54	1.54	1.52
C15—H16	1.10	1.10	1.10	1.10	0.99	1.10	1.10	
C15—H17	1.09	1.09	1.09	1.09	0.99	1.09	1.09	
C15—C18	1.52	1.52	1.52	1.52	1.51	1.52	1.52	1.51
C18—O19	1.22	1.22	1.22	1.21	1.22	1.22	1.22	1.22
C18—C20	1.51	1.51	1.51	1.51	1.50	1.51	1.51	1.50
C20—H	1.10	1.09	1.10	1.09	0.98	1.10	1.09	
C24—H						1.10	1.09	
Bond angle (°)								
C2—C1—C6	119.5	119.4	117.6	117.6	117.1	120.2	120.2	120.1
C2—C1—N11	116.9	117.0	118.9	119.0	117.2	117.3	117.4	116.4
C6—C1—N11	123.6	123.7	123.5	123.5	125.7	122.5	122.5	123.5
C1—C2—C3	120.5	120.5	121.7	121.7	123.4	118.2	118.3	118.0
C1—C2—H24	119.6	119.5						
C3—C2—H24	120.0	120.0						
C1—C2—Cl24			120.0	120.0				
C3—C2—Cl24			118.3	118.3				
C1—C2—C24						121.6	121.6	121.6
C3—C2—C24						120.2	120.2	120.4
C2—C3—C4	120.3	120.3	119.9	119.9	118.8	121.8	121.8	121.7
C2—C3—H7	119.4	119.4	119.1	119.1	120.6	118.5	118.5	
C4—C3—H7	120.3	120.3	121.0	121.0		119.6	119.6	
C3—C4—C5	119.2	119.2	119.3	119.3	119.6	119.2	119.2	119.2
C3—C4—H8	120.4	120.4	119.8	119.8	120.2	120.1	120.2	
C5—C4—H8	120.5	120.5	120.9	120.8	120.2	120.7	120.7	
C4—C5—C6	121.3	121.3	120.9	120.9	120.9	120.6	120.6	120.6
C4—C5—H9	119.9	119.9	120.1	120.1	119.6	120.3	120.3	
C6—C5—H9	118.8	118.8	118.9	118.9	119.6	119.1	119.1	
C1—C6—C5	119.3	119.4	120.6	120.6	120.3	120.0	120.0	120.4
C1—C6—H10	119.7	119.6	118.6	118.5	119.8	119.3	119.2	
C5—C6—H10	121.0	121.0	120.8	120.9	119.8	120.8	120.8	
C1—N11—H12	116.4	116.5	116.7	116.6	118.0	116.8	116.9	
C1—N11—C13	128.8	128.9	128.0	128.2	128.1	128.9	129.0	128.9
H12—N11—C13	114.6	114.4	115.2	115.1	113.9	114.1	113.9	
N11—C13—014	125.7	125.9	125.5	125.7	124.6	125.9	126.2	124.8
N11—C13—C15	115.3	115.1	115.5	115.3	116.3	115.2	115.1	116.2
O14—C13—C15	119.0	118.9	119.0	119.0	119.2	118.8	118.7	119.0
C13—C15—H16	106.7	106.7	106.8	106.9	106.8	106.8	106.8	
C13—C15—H17	106.4	106.4	106.2	106.3	106.8	106.3	106.3	
C13—C15—C18	119.7	119.6	119.2	119.0	122.1	119.3	119.2	122.5
H16—C15—H17	106.2	106.2	106.5	106.5	106.8	106.5	106.4	
H16—C15—C18	106.1	106.0	106.1	106.0	106.8	106.1	106.1	
H17—C15—C18	111.0	111.1	111.3	111.3	106.8	111.2	111.2	
C15—C18—O19	122.1	122.3	121.8	121.9	123.3	121.9	122.1	
C15—C18—C20	116.3	116.2	116.4	116.3	115.8	116.5	116.4	
O19—C18—C20	121.6	121.4	121.9	121.7	123.9	121.7	121.5	121.2
C18—C20—H21	109.2	109.3	109.3	109.4	109.5	109.3	109.4	
C18—C20—H22	110.3	110.2	110.2	110.2	109.5	110.3	110.3	
C18—C20—H23	110.6	110.6	110.6	110.5	109.5	110.6	110.5	
H21—C20—H22	109.6	109.7	109.6	109.7	109.5	109.7	109.7	
H21—C20—H23	106.8	106.7	106.8	106.7	109.5	106.8	106.7	
H22—C20—H23	110.3	110.3	110.2	110.2	109.5	110.3	110.2	

(*continued on next page*)

Table 2 (*continued*)

Structural parameters	AAA		2CAAA		Expt.[a]	2MAAA		Expt.[b]
	B3LYP/6-311++G**	B3LYP/cc-pVTZ	B3LYP/6-311++G**	B3LYP/cc-pVTZ		B3LYP/6-311++G**	B3LYP/cc-pVTZ	
C2—C24—H25						112.0	112.0	
C2—C24—H26						112.3	112.3	
C2—C24—H27						110.4	110.4	
H25—C24—H26						107.1	106.9	
H25—C24—H27						107.4	107.4	
H26—C24—H27						107.5	107.6	

[a] Values taken from Ref. [24].
[b] Values taken from Ref. [25].

using the following relationship derived from the basic theory of Raman scattering [23].

$$I_i = \frac{f(v_0 - v_i)^4 S_i}{v_i[1 - \exp(-hcv_i/kT)]}$$

where v_0 is the exciting frequency (cm^{-1}), v_i is the vibrational wavenumber of the *i*th normal mode, *h*, *c* and *k* are universal constants, and *f* is the suitably chosen common scaling factor for all the peak intensities.

Results and discussion

Structural properties

The optimised geometry and the scheme of atom numbering of AAA, 2CAAA and 2MAAA are represented in Fig. 1. The bond lengths and the bond angles for the optimised geometry of AAA, 2CAAA and 2MAAA at B3LYP levels with 6-311++G** and cc-pVTZ basis sets are presented in Table 2. The C—C and C—H bond lengths are found to be not significantly affected by Cl and —CH_3 substitutions. The bond length of the compounds AAA, 2CAAA and 2MAAA determined at the DFT level of theory are in good agreement with the XRD results [24,25]. All the compounds AAA, 2CAAA and 2MAAA adopt *trans* planar configuration at the amide and non-planar acetyl group however, the nature of the hydrogen bonding defines the orientation of the ketone carbonyl with respect to the amide. An intramolecular hydrogen bonding C=O···H—N is present between the ketone carbonyl and the amide N—H groups. The N···O distance is seen to be 2.77 Å in AAA, 2.79 Å in 2CAAA and 2.79 Å in 2MAAA. The hydrogen bond distance O···H is shorter in AAA (1.95 Å) than that of *o*-substituted compounds. This is due to steric effect of chloro and methyl groups. The substituents do not affect the amide group parameters. The acetyl group (—$COCH_3$) is not planar with respect to anilide part of the molecules. This is confirmed from the dihedral angle C13—C15—C18—C20 and is found to be 144°, 142.2° and 141.2° in AAA, 2CAAA and 2MAAA molecules, respectively.

The bond lengths between the amide nitrogen and the aromatic ring, C1—N11 and between the amide nitrogen and the carbonyl group, N11—C13 given in Table 2 reflect the changes in conjugation. The C1—N11 bond distance slightly increases in 2MAAA than that of AAA and 2CAAA. In 2MAAA the adjacent methyl group influence on the rotation of acylamino group. As the steric hindrance increases and the plane of acylamino group rotates, the C1—N11 bond becomes longer and the N11—C13 bond becomes shorter. The hyperconjugative effect of —CH_3 group on the C1—N11 bond distances is also plays the role. The C2—C1—C6 bond angle is shorter in 2CAAA (117.6°) than that of AAA (119.5°) and 2MAAA (120.2°). This is due to the presence of the —I effect of electron withdrawing —Cl group in 2CAAA.

With the electron donating methyl substituent on the benzene ring of 2MAAA, the symmetry of the ring is distorted, yielding ring angles smaller than 120° at the point of substitution and slightly larger than 120° at the ortho and meta positions [26].

Table 3
The calculated thermodynamic parameters of acetoacetanilide (AAA), 2-chloroacetoacetanilide (2CAAA) and 2-methylacetoacetanilide (2MAAA) employing B3LYP methods with 6-311++G** and cc-pVTZ basis sets.

Thermodynamic parameters (298 K)	AAA			2CAAA	2MAAA	
	B3LYP/6-311++G**	B3LYP/cc-pVTZ	B3LYP/6-311++G**	B3LYP/cc-pVTZ	B3LYP/6-311++G**	B3LYP/cc-pVTZ
SCF energy, (Hartrees)	−593.0793	−593.1282	−1052.6998	−1052.7578	−632.4054	−632.3060
Total energy (thermal), E_{total} (kcal mol^{-1})	128.4	128.6	123.1	123.3	146.7	144.8
Vibrational energy, E_{vib} (kcal mol^{-1})	126.6	126.8	121.3	121.5	145.0	143.0
Zeropoint vibrational energy (kcal mol^{-1})	120.7	120.9	114.7	114.9	138.1	137.8
Heat capacity, C_v (cal mol^{-1} K^{-1})	45.2	45.0	49.0	48.8	51.1	43.9
Entropy, *S* (cal mol^{-1} K^{-1})	112.5	112.2	119.4	119.3	119.9	105.6
Rotational constants (GHz)						
X	1.95	1.95	1.04	1.05	1.41	1.41
Y	0.40	0.40	0.38	0.38	0.39	0.39
Z	0.34	0.34	0.29	0.29	0.31	0.31
Dipolemoment (Debye)						
μ_x	2.88	2.87	−2.18	−2.15	2.97	2.97
μ_y	−1.17	−1.17	−0.05	−0.00	1.65	1.66
μ_z	−0.27	−0.29	−0.13	−0.17	0.30	0.29
μ_{total}	3.12	3.12	2.18	2.16	3.41	3.42
E_{LUMO+1} (eV)	−0.7886	−0.6041	−1.0036	−0.8498	−0.7578	−0.5802
E_{LUMO} (eV)	−1.5209	−1.3328	−1.4779	−1.2874	−1.5206	−1.3443
E_{HOMO} (eV)	−6.2608	−6.1691	−6.4494	−6.3509	−6.1417	−6.0573
E_{HOMO-1} (eV)	−7.0492	−6.9852	−7.0652	−6.9909	−6.7928	−6.7341
$E_{LUMO-HOMO}$ (eV)	4.7400	4.8363	4.9716	5.0635	4.6211	4.7130

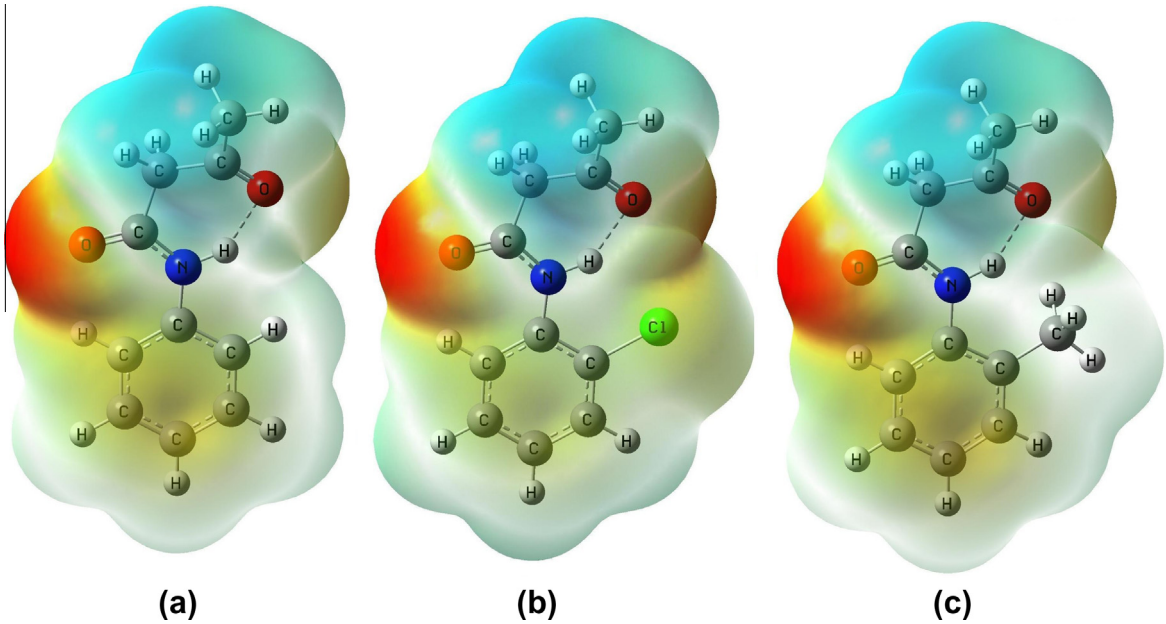

Fig. 2. The total electron density surface mapped with electrostatic potential of (a) acetoacetanilide and (b) 2-chloroacetoacetanilide and (c) 2-methylacetoacetanilide.

The angle at the point of substitution C1—C2—C3 is 118.0° while the bond angle at ortho position to the —CH_3 substitution C2—C3—C4 is 121.7°. Introduction of electron attracting chloro group leads to significant perturbations in the ring, in a reverse manner. The bond angle C1—C2—C3 is 123.4° where the —Cl group is attached while at ortho, C2—C3—C4 position the angle is found to be 118.8°.

The energies and thermodynamic parameters of the compounds AAA, 2CAAA and 2MAAA have also been computed at B3LYP methods with 6-311++G** and cc-pVTZ basis sets and are presented in Table 3. The frequency calculations compute the zero point energies, thermal correction to internal energy, enthalpy, Gibbs free energy and entropy as well as the heat capacity for a molecular system. The calculated SCF energy of the compounds clearly indicates that 2CAAA is more stable than AAA and 2MAAA. From Table 3 it is observed that the dipole moment of 2MAAA is higher than the dipole moments of AAA and 2CAAA due to the presence of the electron donating —CH_3 group.

Determination of molecular electrostatic potential

To understand the relative polarity [27] the molecular electrostatic potential surface (MEP) of the molecular complex has been determined by B3LYP/6-311++G** method [28]. The total electron density mapped with electrostatic potential surface which displays electrostatic potential (electron + nuclei) distribution, molecular shape, size and dipole moments of the molecules AAA, 2CAAA and 2MAAA are shown in Fig. 2. The MEP surface of the compounds is represented in the Supplementary Figure S1 and the electrostatic potential contour map for positive and negative potentials are also shown in Fig. 3.

The electron rich and partially negative charge of the MEP surface is shown in red colour, the blue region reveals the electron deficient and partially positive charge, light blue region shows slightly electron deficient region, the slightly electron rich region is indicated by yellow and the green colour shows neutral. It is obviously from the Figs. 2 and 3 that the region around carbonyl

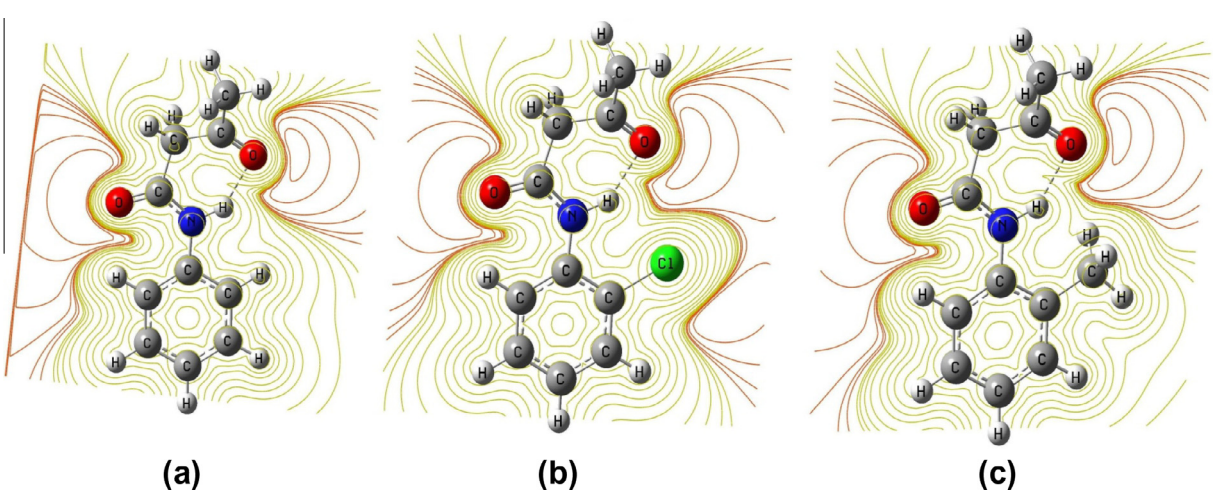

Fig. 3. The contour map of electrostatic potential of the total density of (a) acetoacetanilide and (b) 2-chloroacetoacetanilide and (c) 2-methylacetoacetanilide.

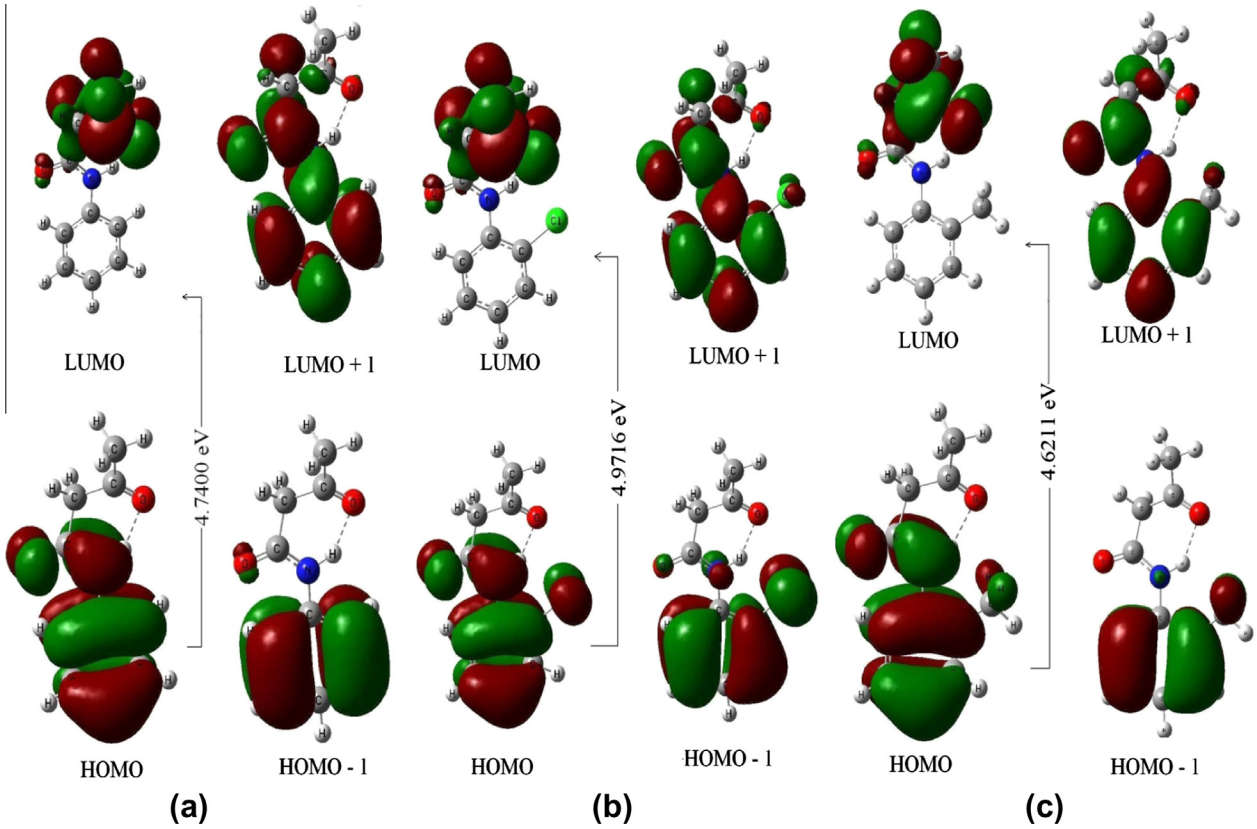

Fig. 4. The frontier molecular orbitals and their energy gap of (a) acetoacetanilide and (b) 2-chloroacetoacetanilide and (c) 2-methylacetoacetanilide.

oxygen atoms represents the most negative potential region (red). The hydrogen atoms attached to the ends of methyl and methylene group posses the maximum bang of positive charge (blue). The predominance of green region in the MEP surfaces corresponds to a potential halfway between the two extremes red and dark blue colour. The total electron density of the molecule 2CAAA ($+4.82e \times 10^{-2}$ to $-4.82e \times 10^{-2}$) is smaller than 2MAAA ($+5.19e \times 10^{-2}$ to $-5.19e \times 10^{-2}$) and AAA ($+5.19e \times 10^{-2}$ to $-5.19e \times 10^{-2}$) is due to the presence of the $-I$ effect of chlorine in 2CAAA.

Analysis of frontier molecular orbitals

Well known concepts such as conjugation, aromaticity and lone pairs are well illustrated by molecular orbitals. The energies of HOMO, LUMO, LUMO + 1 and HOMO – 1 and their orbital energy gap are calculated by using B3LYP/6-311++G** method and the pictorial illustration of the frontier molecular orbitals and their respective positive and negative regions are shown in Fig. 4.

The positive and negative phase is represented in red and green colour, respectively. The region of HOMO and LUMO levels spread over the entire molecule and the calculated energy gap of LUMO–HOMO's explains the ultimate charge transfer interface within the molecule. The frontier orbital energy gap in the case of AAA, 2CAAA and 2MAAA are found to be 4.7400, 4.9716 and 4.6211 eV, respectively.

Topological charge distributions

The natural atomic charges of AAA, 2CAAA and 2MAAA calculated by natural population analysis by using the B3LYP/ 6-311++G** method is presented in Table 4. In all these compounds among the ring carbon atoms C1 has a positive charge while others have negative charge. The positive charge of C1 is due to the attachment of highly electronegative nitrogen atom (N11) to it. In both the 2CAAA and 2MAAA compounds the C2 carbon has less

Table 4
Atomic charges of acetoacetanilide (AAA), 2-chloroacetoacetanilide (2ClAAA) and 2-methylacetoacetanilide (2MAAA) by NBO analysis using B3LYP/6-311++G** method.

Atom	AAA	2CAAA	2MAAA
C1	0.15639	0.13253	0.15560
C2	−0.22686	−0.05765	−0.05134
C3	−0.19120	−0.21407	−0.19290
C4	−0.22181	−0.20670	−0.21444
C5	−0.18430	−0.18754	−0.19270
C6	−0.23020	−0.21521	−0.22434
H7	0.20502	0.22005	0.19938
H8	0.20457	0.20838	0.20328
H9	0.20468	0.20757	0.20396
H10	0.24535	0.25014	0.24513
N11	−0.61846	−0.62860	−0.62693
H12	0.42210	0.43723	0.42779
C13	0.68691	0.69221	0.68842
O14	−0.62062	−0.61555	−0.61883
C15	−0.56419	−0.56267	−0.56358
H16	0.25575	0.25535	0.25486
H17	0.23854	0.23764	0.23781
C18	0.59471	0.59073	0.59416
O19	−0.57907	−0.5669	−0.57926
C20	−0.66708	−0.66617	−0.66678
H21	0.23175	0.23008	0.23173
H22	0.22907	0.22904	0.22861
H23	0.22389	0.22352	0.22414
H24	0.20504		
Cl24		0.00662	
C24			−0.60425
H25			0.21051
H26			0.21588
H27			0.21408

Table 5
Second order perturbation theory analysis of Fock matrix of acetoacetanilide (AAA), 2-chloroacetoacetanilide (2CAAA) and 2-methyl acetoacetanilide (2MAAA) by B3LYP/6-311++G** method.

Donor (i)–acceptor (j) interaction	AAA			2CAAA			2MAAA		
	$E^{(2)a}$ (kJ mol^{-1})	E(j) $-E$(i)[b] (a.u.)	F(i, j)[e] (a.u.)	$E^{(2)a}$ (kJ mol^{-1})	E(j) $-E$(i)[b] (a.u.)	F(i,j)[e] (a.u.)	$E^{(2)a}$ (kJ mol^{-1})	E(j)–E(i)[b] (a.u.)	F(i,j)[e] (a.u.)
σ(C1—C2) → σ*(C1—C6)	4.12	1.27	0.065	4.28	1.28	0.066	4.39	1.26	0.066
σ(C1—C2) → σ*(C2—C3)	2.91	1.29	0.055	3.59	1.30	0.061	3.09	1.28	0.056
σ(C1—C6) → σ*(C1—C2)	4.24	1.26	0.065	5.18	1.24	0.072	4.79	1.25	0.069
π(C1—C6) → π*(C2—C3)	18.76	0.28	0.065	19.82	0.27	0.066	19.67	0.29	0.067
σ(C2—C3) → σ*(C1—C2)	3.12	1.26	0.056	4.05	1.27	0.064	3.51	1.25	0.059
σ(C2—C3) → σ*(C1—N11)	3.70	1.11	0.057	3.50	1.15	0.057	3.89	1.10	0.059
σ(C2—C3) → σ*(C3—C4)	2.78	1.28	0.053	3.24	1.32	0.058	3.25	1.28	0.058
π(C1—C6) → π*(C4—C5)	21.33	0.29	0.070	20.92	0.29	0.070	20.67	0.29	0.069
π(C2—C3) → π*(C1—C6)	20.45	0.28	0.069	19.02	0.30	0.069	19.84	0.28	0.068
π(C2—C3) → π*(C4—C5)	17.81	0.29	0.065	16.36	0.31	0.064	19.37	0.29	0.067
σ(C3—C4) → σ*(C2—C3)	2.79	1.28	0.053	3.76	1.28	0.062	3.70	1.28	0.059
σ(C3—H7) → σ*(C1—C2)	3.86	1.08	0.058	4.67	1.06	0.063	4.46	1.07	0.062
σ(C3—H7) → σ*(C4—C5)	3.56	1.10	0.056	3.39	1.11	0.055	3.56	1.10	0.056
π(C4—C5) → π*(C1—C6)	19.11	0.28	0.066	20.35	0.28	0.068	19.73	0.28	0.067
π(C4—C5) → π*(C2—C3)	22.04	0.28	0.070	23.63	0.26	0.072	20.70	0.28	0.069
σ(C4—H8) → σ*(C2—C3)	3.68	1.10	0.057	3.45	1.09	0.055	3.69	1.10	0.057
σ(C4—H8) → σ*(C5—C6)	3.77	1.10	0.058	3.64	1.11	0.057	3.66	1.10	0.057
σ(C5—C6) → σ*(C1—N11)	4.64	1.10	0.064	4.27	1.12	0.062	4.46	1.10	0.063
σ(C5—H9) → σ*(C1—C6)	3.88	1.08	0.058	4.07	1.07	0.059	3.87	1.08	0.058
σ(C5—H9) → σ*(C3—C4)	3.72	1.09	0.057	3.68	1.10	0.057	3.66	1.10	0.058
σ(C6—H10) → σ*(C1—C2)	4.36	1.07	0.061	4.13	1.05	0.059	4.39	1.06	0.061
σ(C6—H10) → σ*(C4—C5)	3.80	1.09	0.058	3.82	1.10	0.058	3.75	1.10	0.057
σ(N11—H12) → σ*(C1—C6)	3.87	1.22	0.062	3.93	1.22	0.062	3.57	1.23	0.059
σ(N11—H12) → σ*(C13—O14)	5.12	1.25	0.072	4.97	1.26	0.071	5.14	1.26	0.072
σ(C13—C15) → σ*(C1—N11)	4.52	1.06	0.062	4.44	1.06	0.061	4.47	1.05	0.061
σ(C15—H16) → π*(C13—O14)	5.90	0.53	0.053	5.99	0.53	0.054	5.81	0.53	0.053
σ(C15—H16) → π*(C18—O19)	7.66	0.52	0.057	7.46	0.52	0.056	7.52	0.52	0.056
σ(C15—H17) → σ*(C18—O19)	4.44	1.11	0.063	4.46	1.12	0.063	4.51	1.11	0.063
σ(C20—H21) → π*(C18—O19)	6.58	0.52	0.053	6.30	0.53	0.052	6.49	0.52	0.053
σ(C20—H22) → σ*(C15—C18)	3.76	0.89	0.052	3.80	0.89	0.053	3.77	0.89	0.052
n(LP(1)N11) → π*(C1—C6)	33.95	0.30	0.090	35.90	0.29	0.092	32.89	0.30	0.089
n(LP(1)N11) → π*(C13—O14)	64.75	0.27	0.120	62.84	0.27	0.119	64.18	0.27	0.120
n(LP(2)O14) → σ*(N11—C13)	23.74	0.72	0.119	24.24	0.72	0.120	23.73	0.72	0.119
n(LP(2)O14) → σ*(C13—C15)	20.47	0.60	0.101	20.26	0.61	0.101	20.51	0.60	0.101
n(LP(2)O19) → σ*(C15—C18)	18.19	0.67	0.100	18.79	0.66	0.101	18.11	0.67	0.099
n(LP(2)O19) → σ*(C18—C20)	19.47	0.67	0.104	19.77	0.67	0.105	19.49	0.67	0.104

[a] Stabilisation (delocalisation) energy.
[b] Energy difference between i(donor) and j(acceptor) NBO orbitals.
[e] Fock matrix element i and j NBO orbitals. LP – lone pair.

negative charge than that of AAA. This is due to the attachment of chlorine and methyl groups at C2 carbon in 2CAAA and 2MAAA. The very high positive charge resides on the carbonyl carbon atoms C13 and C18 because of the partial polar nature of C=O group. This also leads to more negative charge on the oxygen atoms O14 and O19.

Donor–acceptor interactions

The natural bond orbital (NBO) demonstrates the bonding concepts like atomic charge, Lewis structure, bond type, hybridisation, bond order, charge transfer and resonance possibility. The stabilisation of orbital interaction is proportional to the energy difference

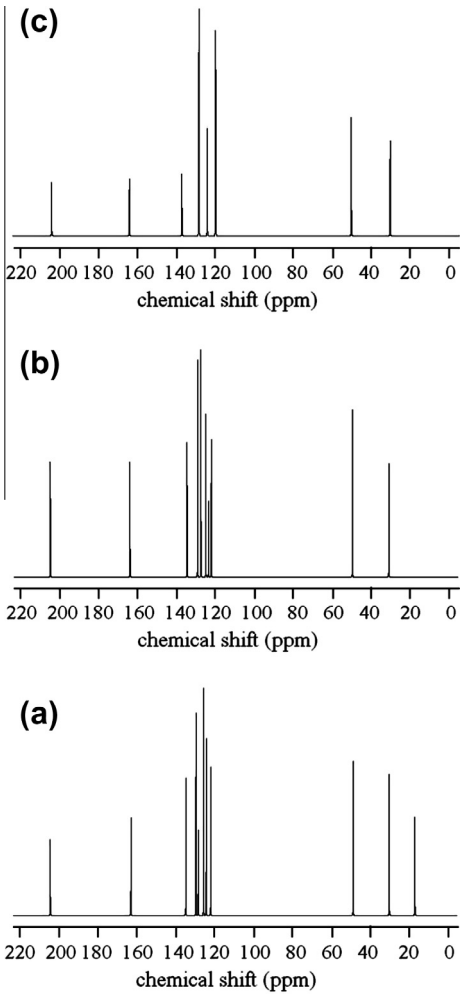

Fig. 5. ^{13}C NMR spectrum of (a) acetoacetanilide and (b) 2-chloroacetoacetanilide and (c) 2-methylacetoacetanilide.

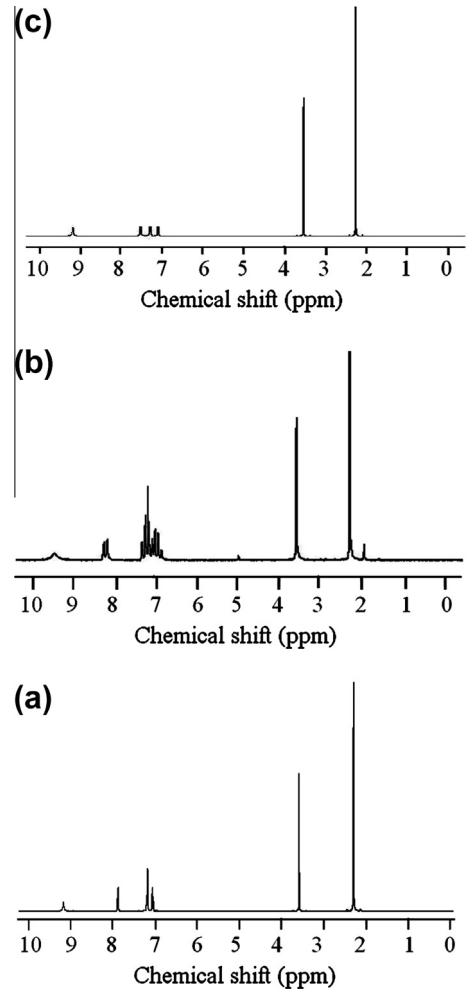

Fig. 6. ^{1}H NMR spectrum of (a) acetoacetanilide and (b) 2-chloroacetoacetanilide and (c) 2-methylacetoacetanilide.

Table 6
The experimental and calculated ^{13}C isotropic chemical shifts (δ_{iso}, ppm) with respect to TMS and isotropic magnetic shielding constants (σ_{iso}) of acetoacetanilde (AAA), 2-chloroacetoacetanilide (2CAAA) and 2-methylacetoacetanilide (2MAAA).

Assignment	AAA			2CAAA			2MAAA		Expt. (δ_{iso})
	σ_{iso} (^{13}C)	Cal. (δ_{iso})	Expt. (δ_{iso})	σ_{iso} (^{13}C)	Cal. (δ_{iso})	Expt. (δ_{iso})	σ_{iso} (^{13}C)	Cal. (δ_{iso})	
C1	36.62	147.91	137.62	35.60	148.93	134.58	38.13	146.4	135.66
C2	60.75	123.78	120.34	60.78	123.75	122.19	50.92	133.61	129.31
C3	49.06	135.47	128.94	49.85	134.68	127.49	47.73	136.8	130.47
C4	54.65	129.88	124.64	52.78	131.75	125.00	55.22	129.31	125.18
C5	48.42	136.11	128.94	44.24	140.29	129.18	51.04	133.49	126.55
C6	59.87	124.66	120.34	46.98	137.55	123.57	60.12	124.41	122.88
C13	15.19	169.34	164.54	18.75	165.78	163.86	15.38	169.15	163.89
C15	131.48	53.05	50.69	129.69	54.84	49.71	130.48	54.05	49.53
C18	−36.52	221.05	204.41	−35.74	220.27	204.66	−36.46	220.99	205.33
C20	148.99	35.54	30.75	149.17	35.36	31.01	148.90	35.63	31.01
C24							163.60	20.93	17.81

between interacting orbitals. Therefore, the interaction having strongest stabilisation takes place between effective donors and effective acceptors. This bonding–anti bonding interaction can be quantitatively described in terms of the NBO approach that is expressed by means of second-order perturbation interaction energy $E^{(2)}$ [29–32]. This energy represents the estimate of the off-diagonal NBO Fock matrix element. The stabilization energy $E^{(2)}$ associated with i(donor) → j(acceptor) delocalisation is estimated from the second-order perturbation approach [33] as given below

$$E^{(2)} = q_i \frac{F^2(i,j)}{\varepsilon_j - \varepsilon_i}$$

where q_i is the donor orbital occupancy, ε_i and ε_j are diagonal elements (orbital energies) and $F(i,j)$ is the off-diagonal Fock matrix element.

The types of donor–acceptor interactions and their stabilisation energies of AAA, 2CAAA and 2MAAA are determined by analysing the Fock matrix and summarised in Table 5. In AAA, 2CAAA and 2MAAA molecules, the lone pair donor orbital, $n_N \rightarrow \pi^*_{CO}$ interaction between the nitrogen lone pair and the C13=O14 antibonding orbital has strong stabilisation of 64.75, 62.84 and 64.18 kJ mol^{-1}, respectively. The lone pair donor orbital, $n_N \rightarrow \pi^*_{CC}$ interaction between the nitrogen lone pair and the C1—C6 antibonding orbital gives stabilisation of 33.95, 35.90 and 32.89 kJ mol^{-1}, respectively. In AAA, 2CAAA and 2MAAA molecules, the bond pair donor orbital, $\pi_{CC} \rightarrow \pi^*_{CC}$ interaction between the C1—C6 bond pair and the C2—C3 antibonding orbital give stabilisation of 18.76, 19.82 and 19.67 kJ mol^{-1} and also the interaction between the C1—C6 bond pair and the C4—C5 antibonding orbital gives more stabilisation with 21.33, 20.92 and 20.67 kJ mol^{-1}.

NMR spectral investigations

NMR spectroscopy is a powerful tool to derive structural information and it involves the change of the spin state of a nuclear magnetic moment when the nucleus absorbs electromagnetic radiation in a strong magnetic field [34]. Thus, NMR techniques are used to detect the presence of particular nuclei in a compound for a given nuclear species. And, it is also an important tool for the identification of molecules and for the examination for their electronic structure [35,36]. The observed ^{13}C and ^{1}H NMR spectra of the compounds AAA, 2CAAA and 2MAAA are given in the Figs. 5 and 6, respectively. The ^{13}C and ^{1}H theoretical and experimental chemical shifts, isotropic shielding constants and the assignments of the compounds AAA, 2CAAA and 2MAAA are presented in Tables 6 and 7. Aromatic carbons give signals with chemical shift values in the range 100–200 ppm [37–39]. The $-I$ effect of nitrogen (N11) reduces the electron density of the carbon atom C1, thus its NMR signal is observed in the downfield at 137.62, 134.58 and 135.66 ppm in the case of AAA, 2CAAA and 2MAAA, respectively. The chemical shift of other ring carbon atoms of AAA, 2CAAA and 2MAAA lie in the range 128.94–120.34, 129.18–122.19 and 129.31–122.88 ppm, respectively. The acetyl methyl group carbon (C20) of all the three molecules gives the NMR absorption at 31 ppm. In 2MAAA the methyl carbon (C24) shows signal at 17.8 ppm. This clearly reveals that the acetyl methyl carbon (C20) atom found in the downfield due to the adjacent highly polar carbonyl group. The methylene group carbon (C15) gives signal in the upfield at around 50 ppm. This is due to the attachment of electron withdrawing nature of the adjacent two carbonyl groups. The acetyl carbonyl carbon atom C18 of AAA, 2CAAA and 2MAAA compounds are significantly observed in the downfield with chemical shift value 204.41, 204.66 and 205.33 ppm while the amide carbonyl carbon atom C13 of AAA, 2CAAA and 2MAAA compounds are observed at 164.54, 163.86 and 163.89 ppm, respectively. This clearly reveals the highly polar nature of acetyl carbonyl group than the amide carbonyl group.

The NMR spectra of the compounds were thoroughly analysed to quantify the possible different effects acting on the shielding constant of protons. In the case of AAA, 2CAAA and 2MAAA compounds the peaks due to —CH_3 and —CH_2— groups appear in the up field regions at 2.29, 1.97, 2.30 and 3.56, 3.63, 3.59 ppm, respectively. The signal of —CH_2— protons is shifted to downfield than that of —CH_3 protons due to electrons withdrawing C=O groups present on either side of —CH_2— group. The NH proton signal of AAA, 2CAAA and 2MAAA compounds appears as a singlet at about 9.20, 9.58 and 9.17 ppm, respectively. The aromatic ring protons produce signal between 7 and 7.5 ppm. The hydrogen atoms present in the benzene ring of AAA and 2MAAA compounds shows NMR peaks in the narrow range 7.11–7.53 and 7.17–7.87 ppm while the 2CAAA shows in the region 5.06–8.32 ppm. A good agreement between the calculated and experimental chemical shift values are observed from Table. 7. The linear regression between the experimental and theoretical ^{1}H and ^{13}C NMR Chemical shifts of AAA, 2CAAA and 2MAAA are represented in Figs. 7 and 8. The correlations of the experimental chemical shift with that of the shielding constants are illustrated in the Supplementary Figs. S2 and S3.

Vibrational analysis

The geometry of AAA, 2CAAA and 2MAAA molecules possessing C_1 point group symmetry. A total of 66 fundamental modes of

Table 7
The Experimental and calculated ^{1}H isotropic chemical shifts (δ_{iso}, ppm) with respect to TMS and isotropic magnetic shielding constants (σ_{iso}) of acetoacetanilde (AAA), 2-chloroacetoacetanilide (2CAAA) and 2-methylacetoacetanilide (2MAAA).

Assignment	AAA			2CAAA			2MAAA		Expt. (δ_{iso})
	σ_{iso} (^{1}H)	Cal. (δ_{iso})	Expt. (δ_{iso})	σ_{iso} (^{1}H)	Cal. (δ_{iso})	Expt. (δ_{iso})	σ_{iso} (^{1}H)	Cal. (δ_{iso})	
H7	24.42	7.55	7.31	24.71	7.26	7.36	24.57	7.4	7.17
H8	24.65	7.32	7.11	24.81	7.16	5.06	24.77	7.2	7.18
H9	24.31	7.66	7.31	24.54	7.43	7.27	24.52	7.45	7.06
H10	23.03	8.94	7.53	25.31	6.66	8.32	22.96	9.01	7.87
H12	22.03	9.94	9.20	22.42	9.55	9.58	22.30	9.67	9.17
H16	28.50	3.47	3.56	28.62	3.53	3.63	28.42	3.55	3.59
H17	28.29	3.68	3.56	28.44	3.53	3.63	28.26	3.71	3.59
H21	29.38	2.59	2.29	29.47	2.5	1.97	29.36	2.61	2.30
H22	29.92	2.05	2.29	30.00	1.97	1.97	29.93	2.04	2.30
H23	29.37	2.60	2.29	29.47	2.5	1.97	29.36	2.61	2.30
H24	24.77	7.20	7.53						
H25							29.44	2.53	2.31
H26							29.32	2.65	2.31
H27							29.62	2.35	2.31

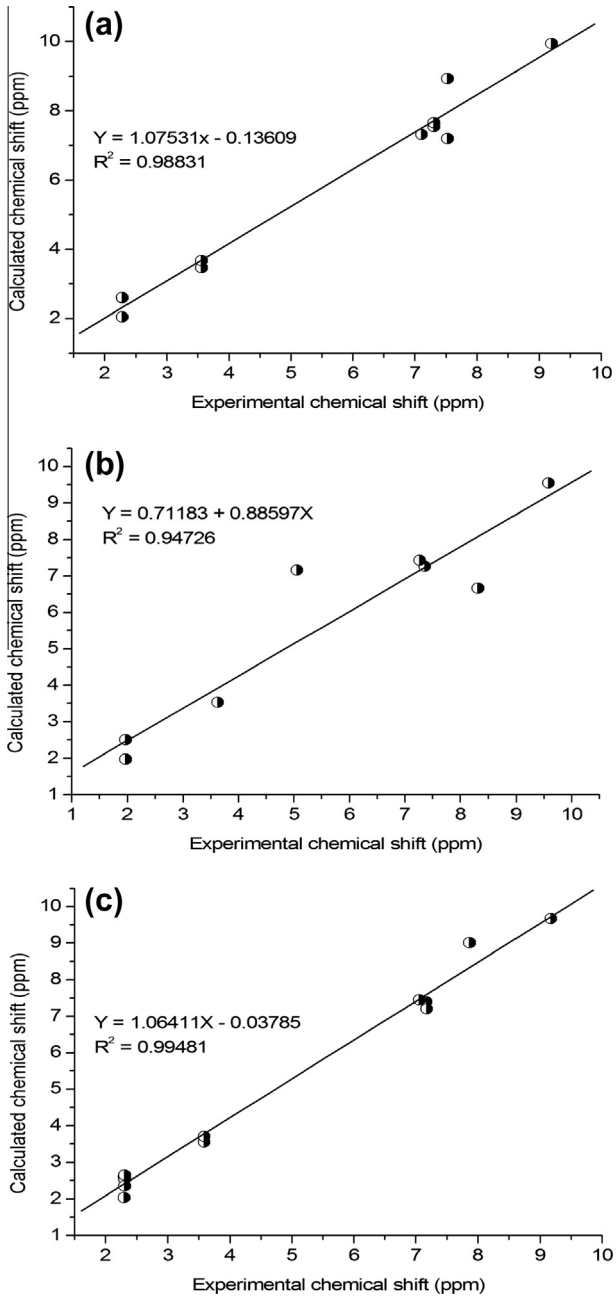

Fig. 7. The linear regression between the experimental and theoretical ^{1}H NMR Chemical shifts (δ) of (a) acetoacetanilide and (b) 2-chloroacetoacetanilide and (c) 2-methylacetoacetanilide.

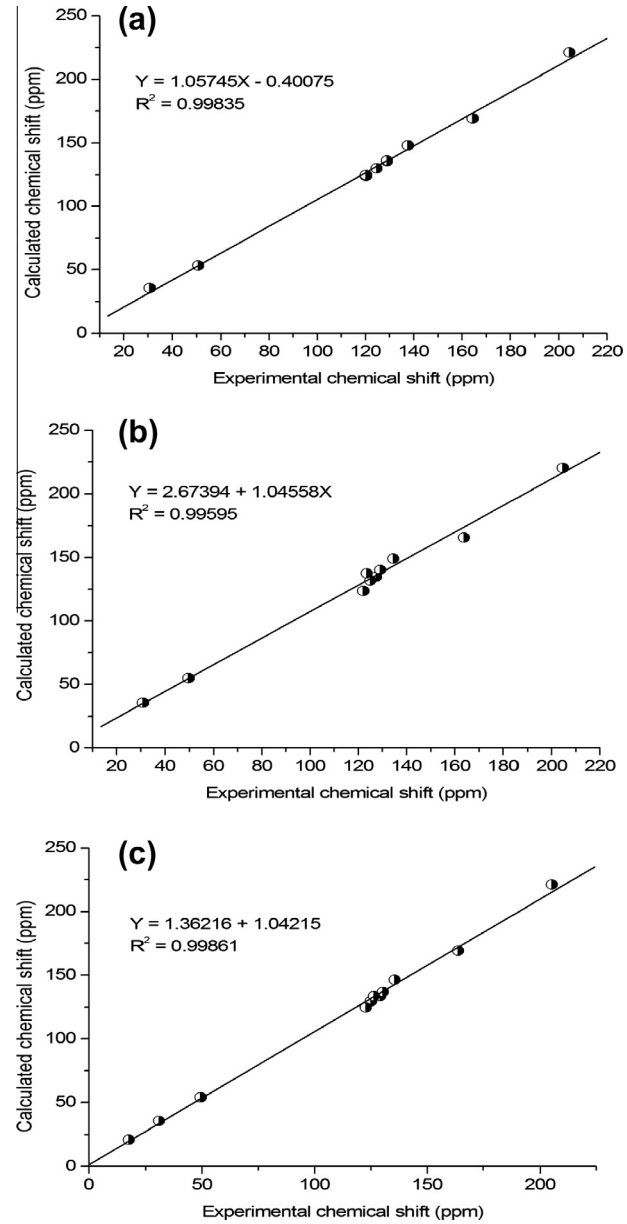

Fig. 8. The linear regression between the experimental and theoretical ^{13}C NMR Chemical shifts (δ) of (a) acetoacetanilide and (b) 2-chloroacetoacetanilide and (c) 2-methylacetoacetanilide.

vibrations are possible for AAA and 2CAAA while 2MAAA produce 75 fundamental modes of vibrations. All the vibrations are active in both IR and Raman. The FTIR and FT-Raman spectra of AAA, 2CAAA and 2MAAA are shown in Figs. 9 and 10, respectively. All the observed wavenumbers are assigned in terms of fundamentals, overtones and combination bands. The observed and calculated frequencies along with their relative intensities and probable assignments are presented in Tables 8–10.

Carbon–carbon vibrations

The carbon–carbon stretching modes of the phenyl group are expected in the range from 1650 to 1200 cm^{-1}. The actual position of these mode are determined not so much by the nature of the substituents but by the form of substitution around the ring [40], although heavy halogens diminish the frequency [41]. In AAA, the ring carbon–carbon stretching bands are appeared in the infrared spectrum at 1619, 1600, 1499, 1446, 1315 and 1161 cm^{-1}. The corresponding C—C stretching modes are observed in the Raman spectrum at 1603, 1501, 1451, 1309 and 1161 cm^{-1}. In the case of 2CAAA the bands observed in the infrared spectrum at 1598, 1594, 1470, 1442, 1281 and 1264 cm^{-1} and 1597, 1593, 1474, 1282 and 1257 cm^{-1} in Raman spectrum are attributed to the corresponding C—C stretching modes. The C—C stretching bands of 2MAAA are observed in the infrared spectrum at 1612, 1550, 1491, 1296 and 1267 cm^{-1} while at 1613, 1545, 1492, 1268 and 1194 cm^{-1} in Raman spectrum. The electron withdrawing nature of chlorine in the ring lowers the C—C stretching vibrations of 2CAAA than that of AAA and 2MAAA. The mode observed at 995 and 1000 cm^{-1} in the IR and Raman spectra is assigned to the trigonal bending of AAA. The mode observed at 991 cm^{-1} in the

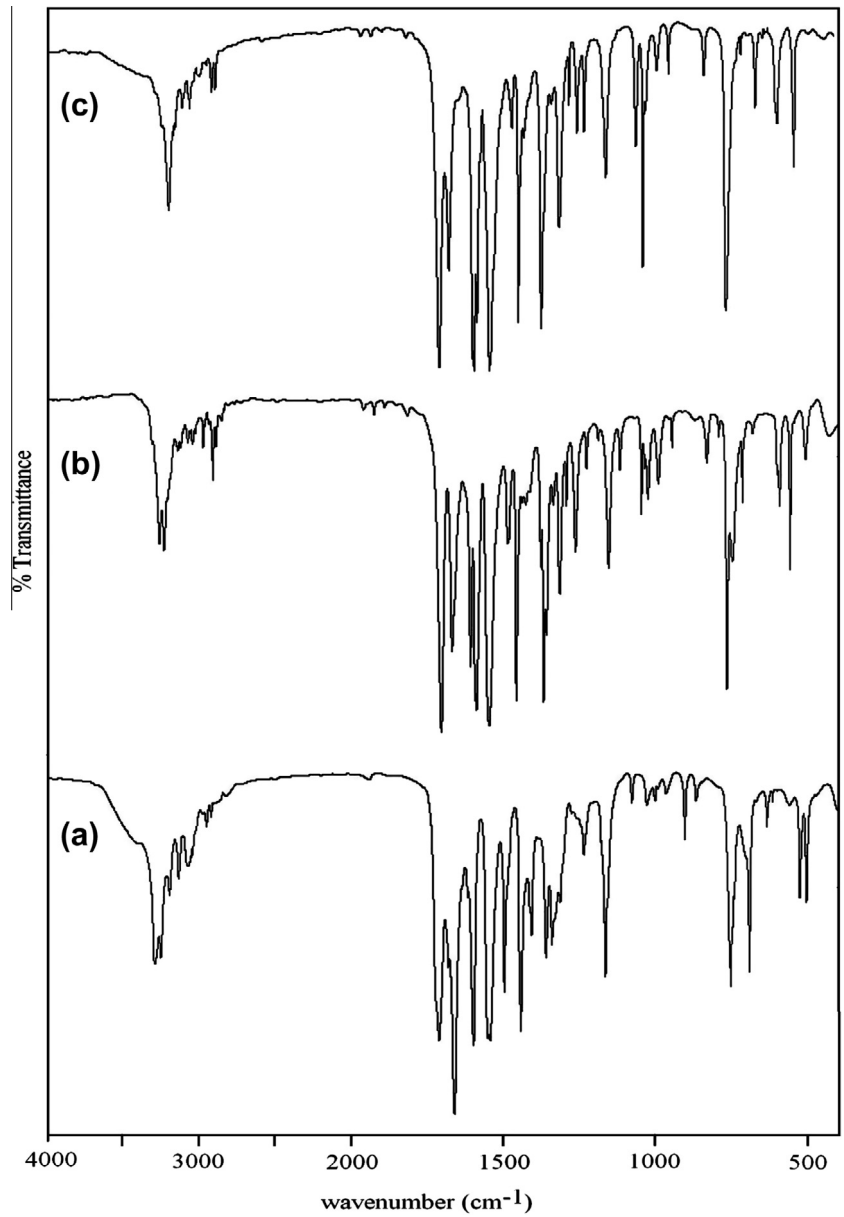

Fig. 9. FTIR spectrum of (a) acetoacetanilide and (b) 2-chloroacetoacetanilide and (c) 2-methylacetoacetanilide.

Raman spectrum is assigned to the trigonal bending of 2CAAA. The trigonal bending mode of 2MAAA is attributed to 994 and 990 cm^{-1} in the IR and Raman spectra, respectively. The observed and calculated CCC in-plane and out of plane bending modes of all the compounds are assigned and presented in Tables 8–10. These results are in good agreement with the literature values [42–45].

C—H vibrations

The aromatic compounds show C—H stretching vibrations in the region 3100–3000 cm^{-1}. In AAA these modes are observed at 3138, 3086, 3072, 3067 and 3046 cm^{-1} in IR spectrum and at 3069, 3059 cm^{-1} in Raman spectrum. The bands observed in the infrared spectra of 2CAAA at 3118, 3080, 3069, 3004 cm^{-1} and at 3080, 3072 cm^{-1} in Raman spectrum are attributed to the corresponding C—H stretching modes. The bands observed in the infrared and Raman spectra of 2MAAA at 3121, 3083, 3049 and 3053 cm^{-1} are assigned to the C—H stretching vibrations. In aromatic compounds the C—H in-plane bending vibrations are observed in the region 1300–850 cm^{-1} and are usually weak. The C—H out of plane bending modes are usually medium intensity [45–48] arises in the region 950–600 cm^{-1}. In the case of AAA the bands observed at 1167, 1155 and 1075 cm^{-1} in IR spectrum are assigned to the C—H in-plane bending vibrations. The C—H in-plane bending modes of 2CAAA are assigned to the wavenumbers at 1150, 1080, 1051, 1037 cm^{-1} in IR and at 1164, 1038 cm^{-1} in Raman spectra. The C—H in-plane bending modes of the compound 2MAAA are also assigned to the wavenumbers at 1049, 1039 cm^{-1} in IR and at 1062 cm^{-1} in Raman spectra. The C—H out of plane bending modes of the compounds are also assigned and presented in the Tables 8–10.

Keto (C=O) group vibrations

The acetyl keto (C=O) stretching vibration is expected in the region 1760–1730 cm^{-1} [48,49]. In AAA the C=O stretching is observed in IR as a strong band at 1713 cm^{-1} and a very weak band at 1715 cm^{-1} in Raman spectra. In 2CAAA, the C=O stretching is

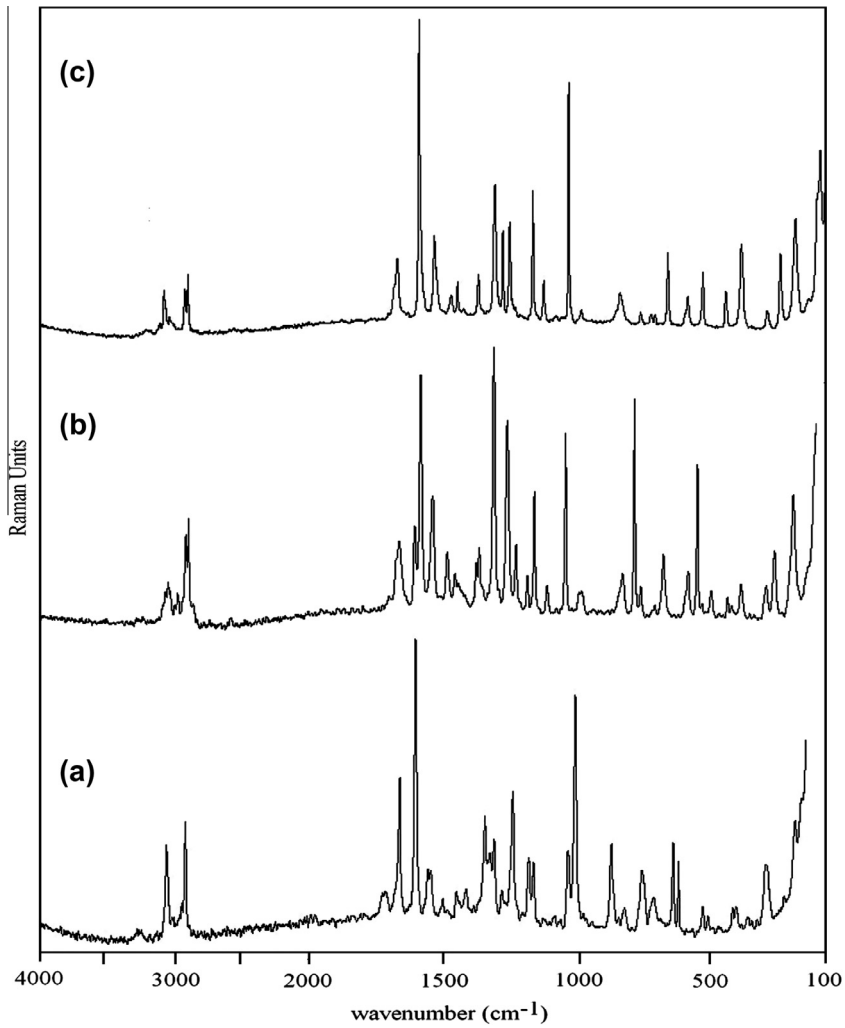

Fig. 10. FT-Raman spectrum of (a) acetoacetanilide and (b) 2-chloroacetoacetanilide and (c) 2-methylacetoacetanilide.

observed in IR as very strong band at 1713 cm^{-1}. In 2MAAA the very strong C=O stretching band is observed in IR at 1708 cm^{-1}. The acetylketo stretching vibration is not at all influenced by the ring substituents. In the present work, the C=O in-plane and out of plane bending vibrations of both the compounds are assigned and given in Tables 8–10.

Amide group vibrations

The characteristic vibrations of the amide (—CONH—) group of AAA, 2CAAA and 2MAAA are analysed and the comparison of the amide (—CONH—) group vibrations are presented in Table 11. The C=O stretching (amide-I band) is found at 1663, 1678 and 1673 cm^{-1} in IR spectrum of AAA, 2CAAA and 2MAAA, respectively. The comparison of the wavenumber of C=O stretching mode in 2CAAA and 2MAAA with that of AAA molecule reveals that the substitution of methyl and chloro group in the phenyl ring does not makes the molecule effectively compete with the carbonyl group and does not show significant variation from that of the parent compound acetoacetanilide [45]. The blue shift of acetyl carbonyl stretching 35–50 cm^{-1} in IR than amide carbonyl stretching is due to the electron donating methyl group. The competition between the delocalisation of the lone pair present in the amide nitrogen towards carbonyl group and the aromatic ring also responsible for the blue shift in acetyl carbonyl stretching frequencies.

The medium band observed at 3294 cm^{-1} in IR is attributed to the N—H stretching of AAA molecule. The molecules 2CAAA and 2MAAA shows the characteristic medium N—H stretching bands at 3206 and 3271 cm^{-1} in the IR spectrum. The influence of the ring substituent on N—H stretching frequency of acetoacetanilide and its derivatives may be the resultant steric effect, direct field effects, hydrogen bonding and bond polarisation effects. The increase in N—H stretching frequency may be expected in introduction of an *o*-methyl or *t*-butyl group into the phenyl ring. In the present investigation, it is observed that there is no rise in the N—H stretching frequency of 2MAAA than that of acetoacetanilide. This clearly confirms that the steric effect due to *o*-methyl group is not significantly operating on the N—H stretching vibration. In 2CAAA, the expected lowering of N—H stretching frequency than AAA is observed. This lowering of N—H stretching frequency in 2CAAA than that of AAA shows the presence of strong intramolecular hydrogen bonding (N11—H12···O19) due to the chlorine atom connected at the *ortho* position. This intramolecular hydrogen bonding is considered to be the predominant effect than the steric and polar factors of chlorine.

The strong vibrations observed at 1545 and 1547 cm^{-1} in IR and Raman spectra are ascribed to the amide-II band, the N—H in-plane bending of AAA. The very strong vibrations observed at 1544 and 1537 cm^{-1} in IR and Raman spectra are ascribed to the amide-II band of 2CAAA. The steric effect due to ortho methyl group significantly operating on the N—H in-plane bending properties. The

Table 8
The observed FTIR, FT-Raman and calculated frequencies by B3LYP method with 6-311++G** and cc-pVTZ basis sets along with their relative intensities and probable assignments of acetoacetanilide[a].

Observed wavenumber (cm^{-1})		B3LYP/6-311++G**				Depolarisation ratio	B3LYP/cc-pVTZ				Depolarisation ratio	Assignment
FTIR	FTR	Unscaled (cm^{-1})	Scaled (cm^{-1})	IR intensity	Raman intensity		Unscaled (cm^{-1})	Scaled (cm^{-1})	IR intensity	Raman intensity		
3294 m		3480	3296	227.96	63.81	0.20	3478	3298	239.13	58.53	0.21	νN—H
3138 w		3240	3140	4.03	17.05	0.16	3245	3142	3.94	16.29	0.19	νC—H
3086 w		3191	3088	17.23	100.00	0.13	3192	3090	19.25	100.00	0.14	νC—H
3072 w	3069 m	3177	3074	21.36	26.13	0.74	3179	3076	23.17	25.99	0.74	νC—H
3067 w	3059 m	3167	3069	1.15	38.17	0.57	3169	3071	1.21	38.63	0.57	νC—H
3046 w		3157	3048	6.55	13.43	0.62	3159	3050	6.76	12.69	0.63	νC—H
2954 vw	2954 w	3144	2956	8.14	28.34	0.63	3144	2958	8.09	27.88	0.63	$\nu_a CH_3$
2921 vw	2927 m	3113	2929	4.39	25.06	0.31	3114	2931	4.79	25.75	0.30	$\nu_a CH_2$
		3084	2901	4.96	22.66	0.71	3084	2903	4.87	22.54	0.71	$\nu_a CH_3$
2853 vw	2863 vw	3028	2855	0.79	78.24	0.01	3031	2857	0.76	67.26	0.01	$\nu_s CH_3$
		3017	2838	1.01	34.47	0.16	3017	2840	0.91	32.72	0.16	$\nu_s CH_2$
1714 s	1727 vw	1765	1714	289.48	0.95	0.14	1771	1716	275.63	0.43	0.27	νC=O(keto)
1663 vs	1662 m	1742	1662	177.96	18.29	0.18	1749	1664	132.60	13.22	0.20	νC=O(anilide)
1619 w		1644	1619	19.40	17.77	0.57	1648	1621	0.86	29.34	0.49	νCC
1600 s	1603 vs	1640	1603	208.53	41.99	0.42	1642	1605	198.41	19.63	0.39	νCC
1545 s	1547 w	1589	1547	358.91	28.33	0.38	1590	1549	369.73	24.19	0.38	βN—H
1499 m	1501 vw	1527	1499	65.50	5.22	0.33	1534	1501	68.99	4.77	0.32	νCC
1446 s	1451 w	1475	1446	43.82	1.97	0.44	1482	1448	54.00	2.28	0.52	νCC
1415 w	1414 w	1474	1415	16.68	3.12	0.75	1476	1417	10.00	2.73	0.75	$\delta_a CH_3$
		1463	1434	17.34	3.36	0.65	1463	1436	16.44	3.31	0.66	$\delta_a CH_3$
1410 m		1441	1410	23.49	3.48	0.72	1441	1412	21.20	3.60	0.69	δCH_2
1363 m		1391	1363	59.38	0.47	0.75	1392	1365	54.38	0.67	0.73	$\delta_s CH_3$
1343 m	1344 m	1357	1343	1.25	1.53	0.53	1363	1345	3.31	0.90	0.66	νC—N
1329 w	1325 w	1350	1325	21.94	11.43	0.21	1349	1327	24.25	12.27	0.24	ωCH_2
1315 w	1309 m	1337	1309	89.40	10.07	0.31	1337	1311	87.47	7.18	0.36	νCC
1238 w	1239 m	1275	1239	92.53	27.90	0.25	1278	1240	85.97	22.61	0.28	νN—C
1178 w	1179 w	1231	1179	72.90	5.18	0.25	1233	1180	80.61	4.35	0.27	τCH_2
1167 m		1203	1167	16.95	2.00	0.20	1205	1168	9.46	3.43	0.17	βCH
1161 m	1161 w	1201	1161	7.48	5.84	0.19	1203	1162	14.27	2.69	0.25	νCC
1155 w		1182	1155	6.47	2.00	0.73	1184	1156	3.86	2.23	0.72	βC—H
1143 w		1179	1143	38.59	1.57	0.32	1180	1144	39.69	1.20	0.35	ωCH_3
1075 vw		1110	1074	13.82	0.71	0.20	1113	1076	12.37	0.70	0.25	βC—H
		1051	1018	3.47	6.74	0.05	1054	1023	2.43	5.04	0.09	βC—H
1028 vw	1034 w	1044	1027	7.41	1.03	0.64	1046	1029	7.00	0.86	0.73	ρCH_3
995 vw	1000 s	1014	994	0.36	21.03	0.10	1020	996	0.39	17.63	0.13	βCCC (TB)
		1001	970	0.65	0.10	0.44	1010	981	0.71	0.14	0.50	βC—H
	976 vw	994	975	20.81	0.30	0.73	995	977	22.12	0.27	0.57	νCC
964 vw		980	963	0.07	0.04	0.70	983	965	0.06	0.03	0.75	τCH_3
906 w		952	905	3.54	0.09	0.47	952	907	3.50	0.06	0.74	γC—H
864 vw	871 w	921	870	8.65	0.02	0.33	927	872	6.75	0.10	0.75	βC=O(anilide)
		904	858	3.49	0.80	0.20	905	861	3.54	0.56	0.28	ρCH_2
754 m	755 w	857	754	3.27	4.11	0.19	859	756	3.34	3.58	0.20	νCC
749 m		848	748	0.88	0.13	0.27	853	750	0.61	0.43	0.38	νCC
743 m		829	742	3.78	1.71	0.13	830	744	3.70	1.53	0.13	βC=O(keto)
693 w		771	692	55.51	0.45	0.75	776	694	39.69	0.15	0.65	γN—H
688 m		761	687	68.96	0.61	0.33	764	689	67.71	0.33	0.47	γC—H
685 m		717	684	3.14	0.79	0.37	719	686	3.55	0.66	0.49	γC—H
636 w	638 m	706	637	21.66	0.02	0.48	711	639	17.22	0.12	0.75	γC—H
		632	561	0.60	1.84	0.71	635	566	0.57	1.66	0.70	γC—H
528 w	528 vw	608	527	4.89	1.44	0.12	609	528	4.06	1.53	0.12	γC=O(anilide)

(*continued on next page*)

Table 8 (*continued*)

Observed wavenumber (cm^{-1})		B3LYP/6-311++G**				Depolarisation ratio	B3LYP/cc-pVTZ				Depolarisation ratio	Assignment
FTIR	FTR	Unscaled (cm^{-1})	Scaled (cm^{-1})	IR intensity	Raman intensity		Unscaled (cm^{-1})	Scaled (cm^{-1})	IR intensity	Raman intensity		
		582	517	8.08	2.18	0.39	583	519	8.46	1.76	0.45	βCCC
515 w	505 vw	532	514	34.97	1.13	0.39	533	515	36.58	1.03	0.44	βC—N
506 w		517	505	11.22	0.10	0.75	521	506	10.08	0.15	0.74	$\beta N—C_6H_5$
		467	443	3.71	0.55	0.35	468	445	3.62	0.55	0.30	γC=O(keto)
	417 vw	418	416	0.01	0.01	0.75	421	417	0.00	0.02	0.70	γC—N
	358 vw	387	357	1.19	0.77	0.33	387	358	1.21	0.67	0.33	βCCC
		347	329	1.92	1.01	0.61	347	330	1.85	0.95	0.60	βCCC
	288 w	289	287	1.85	1.09	0.28	291	288	1.77	1.00	0.27	$\gamma N—C_6H_5$
	224 vw	256	222	0.26	0.33	0.67	259	224	0.26	0.52	0.74	γCCC
	193 w	211	191	14.13	0.27	0.09	211	193	14.35	0.27	0.10	$\beta C—CH_3$
		149	140	0.63	0.09	0.70	152	144	0.38	0.04	0.74	$\gamma C—CH_3$
		111	103	2.83	0.13	0.50	112	106	2.64	0.15	0.52	γCCC
		80	74	2.63	0.73	0.75	81	77	2.54	0.89	0.74	γCCC
		68	63	11.57	0.13	0.71	69	66	9.99	0.12	0.73	γCCC
		43	39	0.71	0.37	0.75	44	42	0.70	0.65	0.75	CH_3 torsion
		29	26	1.02	0.73	0.75	29	29	1.02	0.83	0.75	Lattice vibration

[a] ν – stretching; β – in-plane bending; δ – deformation; ρ – rocking; γ – out of plane bending; ω – wagging; τ – twisting and TB-trigonal bending.

N—H in-plane bending of 2MAAA are ascribed to the strong vibrations observed in the IR and Raman spectra at 1597 and 1590 cm^{-1}. A blue shift of 45–50 cm^{-1} is observed in the amide-II bands of 2MAAA than AAA.

The vibrational modes observed at 1343, 1339 and 1340 cm^{-1} in IR spectra are ascribed to the amide-III band, the C—N stretching mode of AAA, 2CAAA and 2MAAA, respectively. The spectral data indicates that no appreciable rise in C—N stretching frequencies due to the influence of the methyl and chloro groups. The amide-IV, C=O in-plane bending vibration of AAA is found at 864 and 871 cm^{-1} in the IR and Raman spectra. In 2CAAA compound, this mode is observed at 836 and 847 cm^{-1} in the IR and Raman spectra. The amide-IV band of 2MAAA is assigned at 834 and 842 cm^{-1} in the IR and Raman spectra. There is a red shift (~30 cm^{-1}) in the C=O in-plane bending frequencies of 2CAAA and 2MAAA than that of AAA are observed.

The amide-V, the N—H out of plane bending mode of AAA, 2CAAA and 2MAAA are found at 693, 758 and 717 cm^{-1} in the IR spectrum. The substituent effect of chlorine plays significantly and the blue shift in *o*-substituted compounds than the parent in the amide-V vibration is observed. The C=O out of plane bending mode (amide-VI) of AAA is observed at 517 cm^{-1} in IR spectra. The C=O out of plane bending mode of 2CAAA are observed at 593 and 595 cm^{-1} in IR and Raman spectra. The C=O out of plane bending of 2MAAA are assigned at 680 and 689 cm^{-1} in IR and Raman spectra, respectively. A blue shift of amide-VI, C=O out of plane bending modes of 2MAAA and 2CAAA than AAA is observed.

Methyl group vibrations

The asymmetric and symmetric stretching modes of $—CH_3$ group normally appear at about 2965 and 2880 cm^{-1} [50]. The symmetric stretching, $\nu_s(CH_3)$ frequencies are established at 2853 and 2863 cm^{-1} in the infrared and Raman spectra of AAA. The asymmetric stretching, $\nu_a(CH_3)$ frequencies are observed at 2954 cm^{-1} in AAA. The symmetric stretching, $\nu_s(CH_3)$ frequencies are observed at 2883 and 2890 cm^{-1} in the infrared and Raman spectra of 2CAAA. The asymmetric stretching, $\nu_a(CH_3)$ frequencies of 2CAAA are established at 2923 and 2926 cm^{-1} in the infrared and Raman spectra. The symmetric stretching, $\nu_s(CH_3)$ frequencies are assigned to the wavenumber at 2871 and 2874 cm^{-1} in the infrared and Raman spectra of 2MAAA. The asymmetric stretching, $\nu_a(CH_3)$ frequencies are attributed to 2980, 2918, 2898 and 2984, 2921, 2901 cm^{-1} in the infrared and Raman spectra of 2MAAA. The asymmetric methyl deformation modes $\delta_a(CH_3)$ of AAA are observed at 1415 and 1414 cm^{-1} in IR and Raman spectra. The symmetrical methyl deformation modes, $\delta_s(CH_3)$ of AAA are observed at 1363 cm^{-1} in IR spectrum. In 2CAAA, the asymmetrical methyl deformation modes, $\delta_a(CH_3)$ are observed at 1449, 1431 and 1450 cm^{-1} in IR and Raman spectra. The symmetrical methyl deformation modes, $\delta_s(CH_3)$ of 2CAAA are assigned to 1366 and 1368 cm^{-1} in IR and Raman spectra. The asymmetrical methyl deformation modes, $\delta_a(CH_3)$ of 2MAAA are observed at 1486, 1461, 1444, 1430 and 1469, 1451 cm^{-1} in IR and Raman spectra. The symmetrical methyl deformation modes, $\delta_s(CH_3)$ of 2MAAA are attributed to 1372, 1365 and 1373, 1366 cm^{-1} in IR and Raman spectra. The assignment of the bands at 1143 and 1121 cm^{-1} in the infrared spectrum are assigned to the methyl wagging mode of the compounds AAA and 2MAAA, respectively. The band at 1131 cm^{-1} in the Raman spectrum is assigned to the methyl wagging mode of 2CAAA. The methyl twisting mode of the compounds AAA, 2CAAA and 2MAAA are attributed to the bands at 964, 952 and 944 cm^{-1}, respectively in the infrared spectra. The rocking mode of the methyl group of AAA is observed at 1028 and 1034 cm^{-1} in the infrared and Raman spectra, respectively. The corresponding mode of the compound 2CAAA is seen at 1027 and 1035 cm^{-1} in the

Table 9
The observed FTIR, FT-Raman and calculated frequencies by B3LYP method with 6-311++G** and cc-pVTZ basis sets along with their relative intensities and probable assignments of 2-chloroacetoacetanilide[a].

Observed wavenumber (cm^{-1})		B3LYP/6-311++G**				Depolarisation ratio	B3LYP/cc-pVTZ				Depolarisation ratio	Assignment
FTIR	FTR	Unscaled (cm^{-1})	Scaled (cm^{-1})	IR intensity	Raman intensity		Unscaled (cm^{-1})	Scaled (cm^{-1})	IR intensity	Raman intensity		
3206 m		3457	3203	190.69	73.35	0.19	3459	3204	187.19	76.15	0.20	νN—H
3118 w		3244	3115	7.85	25.08	0.16	3249	3116	7.70	27.56	0.19	νC—H
3080 w	3080 vw	3203	3077	5.48	86.79	0.15	3205	3078	6.32	97.89	0.17	νC—H
3069 w	3072 vw	3189	3058	11.46	63.86	0.40	3191	3059	12.72	75.32	0.39	νC—H
3004 w		3174	3001	2.75	29.21	0.71	3176	3002	3.11	34.25	0.70	νC—H
2923 w	2926 vw	3144	2920	7.59	34.08	0.63	3144	2921	7.59	38.86	0.63	$\nu_a CH_3$
2888 w	2903 w	3116	2895	4.41	30.64	0.32	3119	2896	4.83	36.17	0.31	$\nu_a CH_2$
		3083	2864	5.12	28.67	0.71	3082	2864	5.00	33.06	0.72	$\nu_a CH_3$
2883 w	2890 w	3028	2858	0.93	100.00	0.02	3030	2881	0.89	100.00	0.02	$\nu_s CH_3$
		3019	2850	0.65	36.88	0.17	3019	2851	0.56	41.13	0.18	$\nu_s CH_2$
1710 vs		1772	1708	227.17	2.63	0.21	1776	1709	207.91	2.18	0.31	νC=O(keto)
1678 s	1674 w	1744	1676	211.39	21.70	0.18	1751	1677	176.61	17.88	0.20	νC=O(anilide)
1598 vs	1597 vs	1634	1595	145.50	71.40	0.42	1636	1596	102.54	68.34	0.44	νCC
1594 vs	1593 vs	1622	1591	117.53	8.22	0.75	1623	1592	115.57	5.52	0.70	νCC
1544 vs	1537 m	1574	1535	425.78	17.50	0.43	1574	1536	458.68	17.79	0.43	βN—H
1470 m	1474 vw	1498	1468	20.44	6.63	0.39	1503	1469	16.54	7.03	0.34	νCC
1449 w	1450 vw	1474	1447	11.44	3.04	0.73	1475	1448	33.91	2.47	0.51	$\delta_a CH_3$
1442 s		1469	1440	79.49	5.90	0.40	1474	1441	61.58	6.74	0.61	νCC
1431 vw		1462	1429	17.16	4.02	0.64	1463	1430	16.01	4.59	0.66	$\delta_a CH_3$
1372 s		1444	1370	25.67	4.20	0.73	1445	1371	23.81	5.05	0.70	δCH_2
1366 s	1368 w	1390	1364	59.09	0.53	0.75	1391	1365	54.03	0.89	0.73	$\delta_s CH_3$
1339 w		1349	1337	20.04	8.12	0.22	1348	1338	21.25	10.76	0.25	νC—N
1313 m	1312 m	1326	1310	107.76	21.51	0.30	1326	1311	114.48	20.90	0.32	ωCH_2
1281 w	1282 m	1310	1279	18.82	14.19	0.29	1313	1280	9.88	10.40	0.35	νCC
1264 m	1257 m	1267	1255	49.59	18.49	0.22	1269	1256	40.73	17.92	0.23	νCC
1231 m		1235	1229	93.05	3.12	0.42	1236	1230	104.81	3.24	0.45	$\nu N—C_6H_5$
1157 m	1170 m	1202	1168	36.26	1.31	0.42	1204	1169	38.23	1.30	0.37	τCH_2
1150 m	1164 m	1186	1148	1.22	6.50	0.41	1188	1149	1.08	7.06	0.46	βC—H
	1131 vw	1178	1129	38.41	1.65	0.40	1178	1130	35.29	1.59	0.40	ωCH_3
1080 m		1152	1078	0.59	4.15	0.08	1154	1079	0.61	4.50	0.10	βC—H
1051 m		1072	1049	8.37	5.03	0.04	1075	1050	8.45	3.95	0.08	βC—H
1037 s	1038 vs	1051	1035	52.78	15.36	0.10	1056	1036	45.28	16.00	0.14	βC—H
1027 w	1035 vs	1045	1025	6.70	1.06	0.61	1047	1026	6.28	1.03	0.68	ρCH_3
991 w		998	989	0.94	0.04	0.74	1008	990	0.84	0.10	0.74	βCCC(TB)
952 w		995	950	17.41	2.37	0.30	996	951	19.36	2.36	0.25	τCH_3
		960	929	3.42	0.04	0.73	968	939	2.90	0.04	0.75	γC—H
		956	925	2.90	0.29	0.12	956	927	3.08	0.38	0.16	νCC
		905	876	4.29	0.58	0.28	908	881	4.88	0.54	0.37	ρCH_2
836 w	847 vw	879	845	1.21	0.01	0.70	892	847	0.69	0.27	0.74	βC=O(anilide)
		857	829	3.25	4.82	0.21	859	833	2.93	5.03	0.22	νCC
		829	802	3.49	2.32	0.11	830	805	3.48	2.43	0.11	νCC
762 s	769 vw	766	760	24.10	0.21	0.54	772	762	45.99	0.06	0.67	βC=O(keto)
758 w		761	756	102.36	0.88	0.51	759	758	64.27	0.72	0.66	γN—H
		741	717	3.97	0.65	0.29	743	721	2.80	0.68	0.30	γC—H
708 s	712 vw	730	706	0.69	0.21	0.68	739	708	0.59	0.71	0.64	νC—Cl
666 w	669 vs	681	664	14.65	2.69	0.23	683	666	13.66	2.55	0.29	γC—H
600 w		614	598	6.74	1.99	0.25	615	600	5.75	2.26	0.22	γC—H
593 m	595 vw	583	591	8.61	1.90	0.42	584	593	8.09	1.74	0.50	γC=O(anilide)
537 m	539 w	549	535	16.24	2.22	0.35	551	537	12.91	1.64	0.41	βC—N
		544	526	16.92	2.02	0.30	546	530	22.36	2.88	0.33	$\beta N—C_6H_5$
	464 vw	472	462	2.73	0.70	0.37	474	464	3.00	0.86	0.30	γC—N
		454	438	5.55	0.08	0.56	457	443	4.84	0.10	0.67	$\gamma N—C_6H_5$
		445	430	2.19	1.32	0.27	446	433	2.13	1.32	0.32	γC=O(keto)
		393	379	6.63	1.65	0.12	393	381	6.67	1.73	0.14	βCCC
		376	363	1.52	2.26	0.39	376	365	1.56	2.23	0.40	βC—Cl
		299	288	3.00	0.83	0.71	301	292	2.76	0.91	0.69	βCCC
	261 w	281	259	1.28	0.60	0.66	283	261	1.28	0.72	0.73	βCCC
	197 m	243	195	3.05	1.13	0.15	243	197	2.91	1.26	0.14	βCCH_3
		190	182	7.84	0.34	0.75	190	184	7.57	0.40	0.75	γCCH_3
		161	154	2.51	0.62	0.75	163	158	2.80	0.77	0.74	γCCC
	103 w	147	101	0.56	0.12	0.75	148	103	0.55	0.08	0.72	γC—Cl
	81w	104	79	3.33	0.14	0.69	104	81	3.24	0.19	0.71	γCCC
		79	75	2.74	0.95	0.74	79	77	2.53	1.38	0.75	γCCC
		64	60	10.07	0.18	0.74	64	62	8.73	0.20	0.74	γCCC

(*continued on next page*)

Table 9 (*continued*)

Observed wavenumber (cm^{-1})		B3LYP/6-311++G**				Depolarisation ratio	B3LYP/cc-pVTZ				Depolarisation ratio	Assignment
FTIR	FTR	Unscaled (cm^{-1})	Scaled (cm^{-1})	IR intensity	Raman intensity		Unscaled (cm^{-1})	Scaled (cm^{-1})	IR intensity	Raman intensity		
		36	34	1.45	0.17	0.73	35	34	1.34	0.18	0.73	CH_3torsion
		22	20	0.60	0.70	0.75	22	21	0.64	0.94	0.75	Lattice vibration

[a] ν – stretching; β – in-plane bending; δ – deformation; ρ – rocking; γ – out of plane bending; ω – wagging; τ – twisting and TB-trigonal bending.

Table 10
The observed FTIR, FT-Raman and calculated frequencies by B3LYP method with 6-311++G** and cc-pVTZ basis sets along with their relative intensities and probable assignments of 2-methylacetoacetanilide.[a]

Observed wavenumber (cm^{-1})		B3LYP/6-311++G**				Depolarisation ratio	B3LYP/cc-pVTZ				Depolarisation ratio	Assignment
FTIR	FTR	Unscaled (cm^{-1})	Scaled (cm^{-1})	IR intensity	Raman intensity		Unscaled (cm^{-1})	Scaled (cm^{-1})	IR intensity	Raman intensity		
3271 m		3502	3264	183.65	60.17	0.18	3502	3265	190.30	53.58	0.20	νN—H
3121 w		3243	3115	5.03	20.22	0.16	3247	3116	4.98	19.26	0.19	νC—H
3083 vw		3187	3077	22.33	100.00	0.16	3189	3078	24.56	100.00	0.17	νC—H
3049 vw	3053 w	3171	3043	15.21	36.28	0.74	3173	3044	15.99	35.80	0.74	νC—H
		3158	3026	6.81	30.91	0.49	3160	3024	7.10	29.58	0.50	νC—H
2980 w	2984 w	3144	2979	8.20	30.35	0.63	3144	2979	8.10	29.38	0.64	$\nu_a CH_3$(Ac)
2944 w		3117	2939	4.59	27.44	0.32	3119	2939	4.97	27.93	0.31	$\nu_a CH_2$
		3108	2948	18.45	26.58	0.60	3109	2928	17.46	25.05	0.60	$\nu_a CH_3$
2918 w	2921 m	3083	2916	4.86	25.47	0.71	3083	2916	4.75	25.12	0.71	$\nu_a CH_3$(Ac)
2898 w	2901 m	3060	2896	13.61	25.83	0.72	3059	2896	14.05	24.00	0.70	$\nu_a CH_3$
2871 w	2874 w	3028	2869	0.80	88.74	0.02	3030	2869	0.74	74.93	0.02	$\nu_s CH_3$(Ac)
2856 w	2865 w	3019	2860	0.95	35.45	0.17	3019	2860	0.94	35.10	0.16	$\nu_s CH_2$
		3015	2859	21.61	76.09	0.03	3017	2846	20.89	67.10	0.03	$\nu_s CH_3$
1708 vs		1765	1708	287.26	1.28	0.16	1770	1706	278.52	0.69	0.31	νC=O(keto)
1673 s	1670 m	1743	1673	175.90	20.79	0.19	1750	1671	128.59	15.19	0.21	νC=O(anilide)
1612 s	1613 w	1650	1612	45.85	13.02	0.74	1653	1610	31.87	12.29	0.72	νCC
1597 s	1590 s	1630	1590	187.72	54.16	0.41	1632	1588	172.66	40.84	0.39	βN—H
1550 vs	1545 m	1585	1545	336.71	16.26	0.44	1587	1543	351.03	14.21	0.44	νCC
1491 m	1492 w	1519	1492	38.18	7.62	0.38	1523	1489	32.03	6.94	0.34	νCC
1486 m		1494	1487	60.55	3.35	0.75	1498	1484	94.09	3.40	0.72	$\delta_a CH_3$
1461 s	1469 vw	1493	1462	30.81	3.37	0.75	1494	1459	9.16	2.97	0.75	$\delta_a CH_3$
1444 w	1451 vw	1476	1445	10.37	3.82	0.29	1481	1442	5.93	2.88	0.32	$\delta_a CH_3$ (Ac)
1430 w		1474	1431	12.11	2.81	0.75	1475	1428	9.35	2.89	0.75	$\delta_a CH_3$ (Ac)
1380 s	1384 w	1462	1385	16.62	3.50	0.65	1463	1382	16.06	3.49	0.66	δCH_2
1372 s	1373 w	1444	1374	23.94	3.78	0.72	1444	1371	21.62	3.88	0.69	$\delta_s CH_3$
1365 m	1366 w	1420	1367	2.83	3.65	0.53	1423	1364	2.40	3.37	0.50	$\delta_s CH_3$ (Ac)
1340 w		1390	1341	58.89	0.52	0.75	1392	1338	54.02	0.75	0.73	νC—N
1318 m	1319 vs	1349	1319	16.51	11.89	0.20	1348	1316	17.75	12.06	0.22	ωCH_2
1296 w		1335	1298	56.46	8.49	0.32	1335	1295	50.27	5.27	0.38	νCC
		1320	1282	28.79	5.56	0.23	1325	1269	35.85	4.76	0.26	νCC
1267 m	1268 s	1277	1269	104.30	40.66	0.22	1279	1266	99.82	31.79	0.26	νCC
1231 w	1236 w	1231	1233	80.49	7.20	0.27	1232	1230	87.36	6.28	0.30	$\nu N—C_6H_5$
	1194 w	1211	1196	0.48	2.33	0.11	1213	1193	1.19	1.75	0.17	νCC
1158 m	1168 m	1202	1170	28.60	1.15	0.53	1203	1167	26.58	1.00	0.46	τCH_2
		1186	1152	1.09	4.29	0.58	1188	1131	0.80	4.41	0.60	βC—H
1121 w	1122 w	1179	1124	36.83	1.22	0.40	1179	1121	35.74	0.99	0.40	ωCH_3
		1136	1104	3.48	1.71	0.09	1140	1094	2.69	1.52	0.09	ωCH_3
1049 m	1062 s	1073	1052	13.04	12.77	0.08	1076	1048	11.31	9.94	0.12	βC—H
1039 w		1058	1042	1.65	0.06	0.65	1062	1038	1.43	0.08	0.75	βC—H
1028 w		1044	1031	6.96	1.07	0.69	1046	1027	6.64	0.94	0.74	ρCH_3
994 w	990 w	1009	993	1.84	0.86	0.33	1012	989	1.85	0.59	0.43	βCCC(TB)
985 w		996	988	0.68	0.10	0.45	1004	984	0.56	0.10	0.75	ρCH_3(Ac)
		995	968	24.87	2.42	0.18	996	962	26.07	2.22	0.15	τCH_3
		957	950	2.88	0.04	0.70	961	948	2.25	0.01	0.75	βC—H
944 w		954	947	4.36	0.97	0.09	954	943	4.40	0.95	0.11	τCH_3(Ac)
		907	883	3.67	0.24	0.63	909	877	3.87	0.17	0.73	ρCH_2
834 w	842 w	883	845	1.29	0.03	0.73	890	841	0.98	0.23	0.75	βC=O(anilide)

Table 10 (*continued*)

Observed wavenumber (cm^{-1})		B3LYP/6-311++G**				Depolarisation ratio	B3LYP/cc-pVTZ				Depolarisation ratio	Assignment
FTIR	FTR	Unscaled (cm^{-1})	Scaled (cm^{-1})	IR intensity	Raman intensity		Unscaled (cm^{-1})	Scaled (cm^{-1})	IR intensity	Raman intensity		
		856	833	2.07	2.64	0.42	858	834	1.81	2.33	0.40	νCC
	797 s	829	801	3.13	2.17	0.11	830	797	3.33	1.85	0.12	νCC
768 s	774 w	803	772	0.59	6.07	0.06	805	768	0.65	5.28	0.08	γC—H
750 m		769	754	54.11	0.36	0.75	775	750	41.66	0.05	0.66	βC=O(keto)
717 w	714 w	741	721	36.68	0.58	0.37	747	717	36.81	0.40	0.46	γN—H
680 vw	689 w	734	693	30.14	0.20	0.55	741	689	25.14	0.16	0.60	γC=O(anilide)
602 w		703	606	2.43	2.20	0.23	705	602	2.50	1.79	0.32	γC—H
595 w	598 w	616	599	3.88	1.82	0.39	617	595	3.11	1.65	0.34	γC—H
560 m	566 m	584	570	4.38	0.99	0.61	587	566	3.71	0.81	0.70	γC—H
		565	553	23.82	5.62	0.23	567	548	24.51	4.99	0.26	βCCC
501 w	512 w	545	517	1.95	0.17	0.74	550	512	1.93	0.09	0.66	βC—N
		518	507	16.12	0.74	0.39	519	502	17.00	0.64	0.45	βNC_6H_5
		474	465	2.48	0.68	0.39	475	453	2.64	0.72	0.32	βCCC
	452 w	453	457	5.31	0.06	0.36	456	452	4.44	0.09	0.68	γC—N
	401 w	428	406	2.05	0.27	0.30	430	401	2.17	0.26	0.28	γC=O(keto)
		381	375	0.56	1.14	0.55	381	369	0.51	0.98	0.58	$\gamma N—C_6H_5$
	308 w	308	314	3.50	0.80	0.75	310	309	3.24	0.74	0.74	βCCC
	282 w	288	288	2.09	0.44	0.69	290	283	2.16	0.66	0.67	$\beta C—CH_3$
	212 w	270	218	1.41	1.20	0.12	271	213	1.46	1.08	0.11	$\beta C—CH_3$
	201 m	208	207	9.60	0.25	0.48	207	202	9.53	0.24	0.50	$\gamma C—CH_3$
	145 w	182	151	2.36	0.65	0.74	184	146	2.27	0.60	0.73	$\gamma C—CH_3$
	134 w	178	140	0.74	0.03	0.13	182	135	0.74	0.04	0.34	γCCC
	126 m	152	132	0.33	0.09	0.75	156	127	0.23	0.05	0.73	γCCC
		111	114	2.56	0.05	0.59	112	110	2.46	0.06	0.55	γCCC
		77	81	3.09	0.75	0.75	79	78	2.53	0.95	0.75	γCCC
		66	71	10.68	0.15	0.74	67	66	9.52	0.10	0.74	CH_3 Torsion
		36	42	1.30	0.17	0.73	37	37	1.28	0.21	0.73	CH_3 Torsion
		22	28	0.41	0.73	0.75	23	23	0.40	0.87	0.75	Lattice vibration

[a] ν – stretching; β – in-plane bending; δ – deformation; ρ – rocking; γ – out of plane bending; ω–wagging; τ–twisting; Ac-acetyl and TB-trigonal bending.

Table 11
Comparison of FTIR and FT-Raman (FTR) amide (—CONH—) group vibrations of acetoacetanilide (AAA), 2-chloroacetoacetanilide (2CAAA) and 2-methylacetoacetanilide (2MAAA).

Compound name	$\nu_{C=O}$		β_{N-H}		ν_{C-N}		$\beta_{C=O}$		γ_{N-H}		$\gamma_{C=O}$		ν_{N-H}	
	FTIR	FTR	FTIR	FTR	FTIR	FTR	FTIR	FTR	FTIR	FTR	FTIR	FTR	FTIR	FTR
AAA	1663	1662	1545	1547	1343	1344	864	871	693	_	528	528	3294	_
2CAAA	1678	1674	1544	1537	1339	_	836	847	758	_	593	595	3206	_
2MAAA	1673	1670	1590	1597	1340	_	834	842	717	714	680	689	3271	–

infrared and Raman spectra, respectively. The methyl rocking mode of 2MAAA is attributed to the bands observed at 1028 and 985 cm^{-1} in the infrared spectrum. These assignments are agreed well with the reported literatures [51,52].

Methylene group vibrations

The asymmetric and symmetric methylene stretching vibrations normally occur at 2926 and 2853 cm^{-1} [49]. The symmetric stretching, $\nu_s(CH_2)$ frequencies are calculated at 2838 cm^{-1} of AAA. The asymmetric stretching, $\nu_a(CH_2)$ frequencies are established at 2921 and 2927 cm^{-1} in the infrared and Raman spectra of AAA. The $\nu_s(CH_2)$ frequencies are calculated at 2850 cm^{-1} of 2CAAA. The asymmetric stretching, $\nu_a(CH_2)$ frequency is established at 2888 and 2903 cm^{-1} in the infrared and Raman spectra of 2CAAA. The symmetric stretching, $\nu_s(CH_2)$ frequency is assigned to 2944 cm^{-1} in the infrared spectrum of 2MAAA. The $\nu_a(CH_2)$ frequency is attributed to 2856 and 2865 cm^{-1} in the infrared and Raman spectra of 2MAAA. The methylene deformation modes, $\delta(CH_2)$ of AAA, 2CAAA and 2MAAA are observed at 1363, 1372 and 1372 cm^{-1}, respectively in IR spectra. The other methylene wagging, twisting and rocking modes of AAA, 2CAAA and 2MAAA are all given in the Tables 8–10.

C—Cl vibrations

The C—Cl absorption is observed in the broad region between 850 and 550 cm^{-1}. The strong band in IR at 708 cm^{-1} having very weak Raman counterpart at 712 cm^{-1} is assigned to the C—Cl stretching mode of 2CAAA. The in-plane C—Cl deformation vibrations of 2CAAA is calculated at 363 cm^{-1} by B3LYP/6-311++G** method. The out of plane C—Cl mode is assigned and given in the Table 9. These assignments are in good agreement with the literature values [53–55].

Scale factors

A better agreement between the computed and experimental frequencies can be obtained by using scale factors. The method of linear scaling equation is used [56,57] to determine the scaled wavenumbers. The scaling equations were minimised the residual separating experimental and theoretically predicted vibrational frequencies

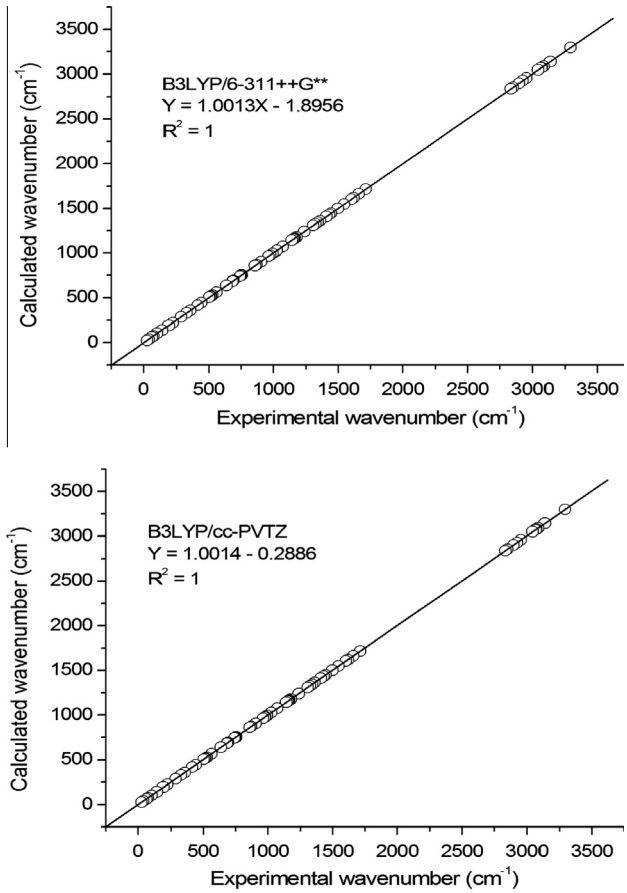

Fig. 11. The linear regression between the experimental and scaled theoretical wavenumbers of acetoacetanilide.

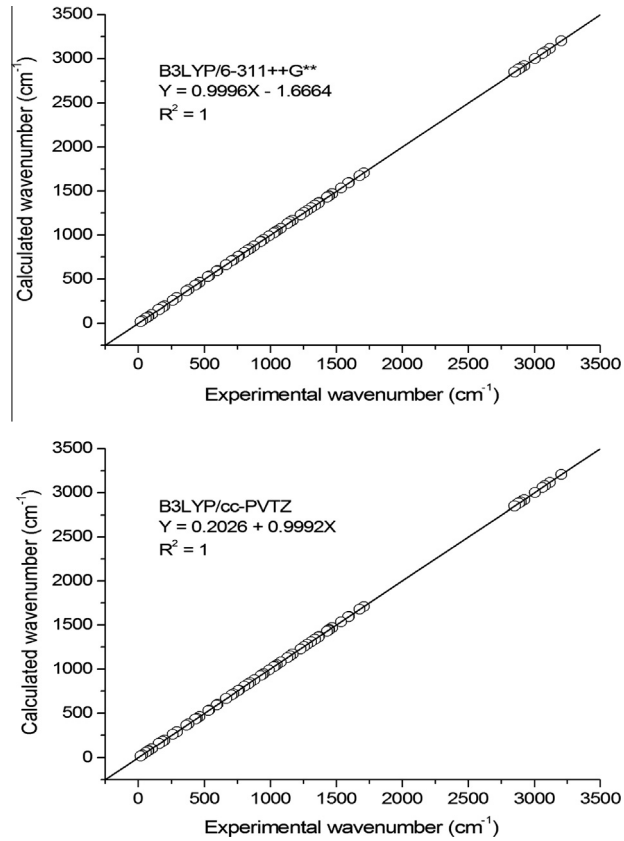

Fig. 12. The linear regression between the experimental and scaled theoretical wavenumbers of 2-chloroacetoacetanilide.

$$\Delta = \sum_{i}^{N}\left(\lambda\omega_i^{Theor} - \nu_i^{Expt}\right)^2$$

where ω_i^{Theo} and ν_i^{Expt} are the *i*th theoretical harmonic frequency and *i*th experimental fundamental frequency (in cm^{-1}), respectively and *N* is the number of frequencies which leads to minimum RMS deviation by the relation

$$RMS = \sqrt{\frac{\Delta}{N}}$$

The scaling equations $y = 1.0018x - 1.7969$ and $y = 1.0014x - 0.2429$ were used to calculate the scaled wave numbers in B3LYP method with 6-311++G** and cc-pVTZ basis sets of AAA, respectively. The scaling equations $y = 0.9996x - 1.4826$ and $y = 0.1526 + 0.9993x$ were used to calculate the scaled wave numbers in B3LYP method with 6-311++G** and cc-pVTZ basis sets of 2CAAA, respectively. The scaling equations $y = 6.8043 + 0.9959x$ and $y = 1.1574 + 0.9980x$ were used to calculate the scaled wave numbers with 6-311++G** and cc-pVTZ basis sets of 2MAAA, respectively. The correlation diagram for the calculated and the experimental frequencies of AAA, 2CAAA and 2MAAA are shown in Figs. 11–13.

Conclusion

Complete structural, vibrational, NMR and DFT analyses of acetoacetanilide, 2-chloroacetoacetanilide and 2-methylacetoacetanilide were carried out and the following observations are made

(i) In 2MAAA the adjacent methyl group influence on the rotation of acylamino group. As the steric hindrance increases, the plane of acylamino group rotates which render the C1—N11 bond becomes longer by (0.06 Å) than N11—C13 bond.

(ii) The *–I* effect of nitrogen (N11) reduces the electron density of the carbon atom C1, thus its NMR signal is observed in the very downfield at 137.62, 134.58 and 135.66 ppm in the case of AAA, 2CAAA and 2MAAA, respectively.

(iii) The acetyl carbonyl carbon atom C18 of AAA, 2CAAA and 2MAAA compounds are significantly observed in the downfield with chemical shift value 204.41, 204.66 and 205.33 ppm while the amide carbonyl carbon atom C13 of AAA, 2CAAA and 2MAAA compounds are also observed in the downfield with chemical shift value of 164.54, 163.86 and 163.89 ppm, respectively. This clearly reveals that acetyl carbonyl group is highly polar than that of amide carbonyl group.

(iv) Substitution of electron withdrawing chloro group in the ring diminished the carbon–carbon stretching frequencies in the case of 2-chloroacetoacetanilide than AAA and 2MAAA. There is no systematic variation in these stretching vibrations with the chloro and methyl group substitution in the ring.

(v) The comparison of the wavenumber of C=O stretching in 2CAAA and 2MAAA with that of AAA molecule reveals that the substitution of methyl and chloro group in the phenyl ring does not makes the molecule effectively compete with the carbonyl oxygen of the amide group. It is evident from the IR and Raman vibrational frequencies of 2CAAA and 2MAAA, that the C=O stretching frequencies of the

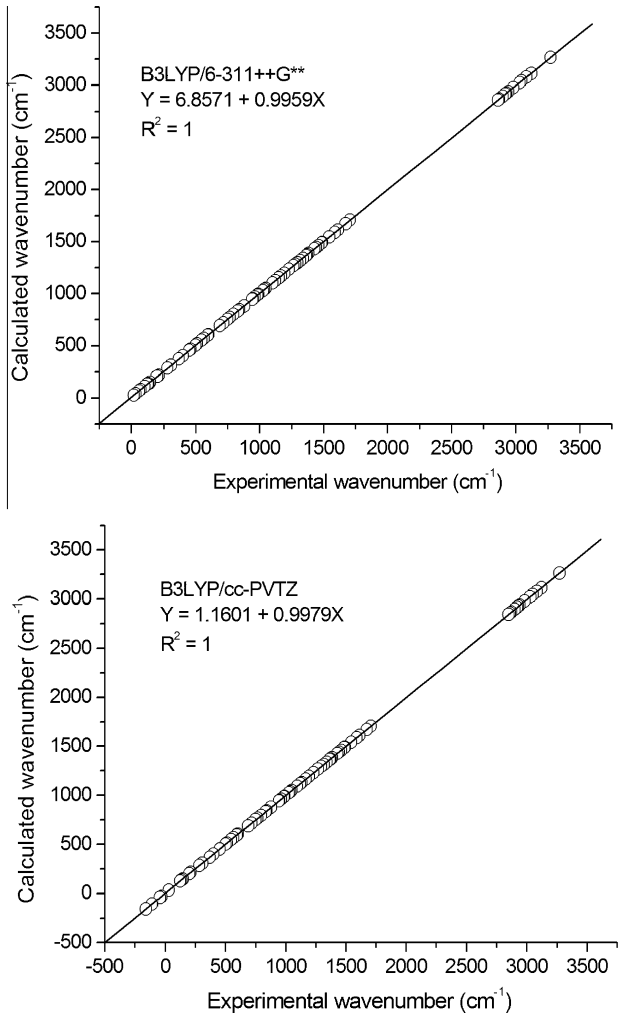

Fig. 13. The linear regression between the experimental and scaled theoretical wavenumbers of 2-methylacetoacetanilide.

compounds 2CAAA and 2MAAA does not show significant variation from that of the parent compound acetoacetanilide.

(vi) It is observed that there is no increase in the N—H stretching frequency of 2MAAA than that of acetoacetanilide. This clearly confirms that the steric effect due to *o*-methyl group is not significantly operating on the N—H stretching vibration. In 2CAAA, the expected red shift of N—H stretching frequency is observed. This lowering of N—H frequency in 2CAAA than that of AAA shows the presence of strong intramolecular hydrogen bonding C=O···H—N between the acetyl carbonyl group and the hydrogen of the amide group due to the chlorine atom connected at the *ortho* position. This intramolecular hydrogen bonding is considered to be the predominant effect than the steric and polar factors of chlorine.

(vii) The blue shift in amide-II band of 2MAAA is observed by 45–50 cm^{-1} than that of AAA. The steric effect due to ortho methyl group significantly operating on the N—H in-plane bending properties.

(viii) The amide-III, the C—N stretching mode of methyl and chloro substituted acetoacetanilide compounds are not affected by the substitution while the amide-V band, the N—H out of plane bending mode of 2-chloroacetoacetanilide compound is shifted to a higher frequency than that of AAA. The substituent effect of chlorine plays significantly and the blue shift in *o*-substituted compounds than the parent in the amide-V vibration is observed.

(ix) The amide-VI, C=O out of plane bending modes of 2MAAA and 2CAAA are significantly raised than that of AAA. A blue shift of amide-VI, C=O out of plane bending modes of 2MAAA and 2CAAA than AAA is observed.

(x) In AAA, 2CAAA and 2MAAA molecules, the $n_N \rightarrow \pi^*_{CO}$ interaction between the nitrogen lone pair and the amide carbonyl (C13=O14) antibonding orbital gives strong stabilisation of 64.75, 62.84 and 64.18 kJ mol^{-1}, respectively.

Appendix A. Supplementary material

Supplementary data associated with this article can be found, in the online version, at http://dx.doi.org/10.1016/j.saa.2013.06.003.

References

[1] M.M. Khater, M.A. Zayed, F.A. Nour–El–Dien, Anal. Bioanal. Chem. 301 (1980) 26.
[2] A.J. Heeger, J. Orenstein, D.R. Ulrich (Eds.), Mater. Res. Soc. Symp. Proc. (1988) 109.
[3] P.N. Prassad, D.J. Williams, Introduction to Nonlinear Optical Effects in Molecules and Polymers, Wiley, New York, 1991.
[4] U. Caruso, M. Casalboni, A. Fort, M. Fusco, B. Panunzi, A. Quatela, A. Roviello, F. Sarcinelli, Opt. Mater. 27 (2005) 1800–1810.
[5] C.–Y. Zhao, Y. Zhang, W.–H. Fang, X.–Z. You, J. Mol. Struct. (Theochem) 367 (1996) 73–81.
[6] D.S. Chemla, J. Zyss (Eds.), Nonlinear Optical Properties of Organic Molecules and Crystals, vols. 1 and 2, Academic Press, New York, 1987.
[7] J.F. Nicoud, Mol. Cryst. Liq. Cryst. 156 (1988) 257–268.
[8] S.G. Prabhu, P. Mohan Rao, J. Cryst. Growth 210 (2000) 824–827.
[9] J. Krc Jr., W.C. McCrone, Anal. Chem. 22 (1950) 845.
[10] N. Vijayan, R. Ramesh Babu, R. Gopalakrishnan, P. Ramasamy, J. Cryst. Growth. 267 (2004) 646–653.
[11] C. Ravikumar, I. Hubert Joe, D. Sajan, J. Chem. Phys. 369 (2010) 1–7.
[12] J.S. Witzeman, W.D. Nottingham, J. Org. Chem. 56 (1991) 1713–1718.
[13] P. Hohenberg, W. Kohn, Phys. Rev. B 136 (1964) 864–871.
[14] A.D. Becke, J. Chem. Phys. 98 (1993) 5648–5652.
[15] A.D. Becke, Phys. Rev. A 38 (1988) 3098–3100.
[16] C. Lee, W. Yang, R.G. Parr, Phys. Rev. B 37 (1988) 785–789.
[17] M.J. Frisch, G.W. Trucks, H.B. Schlegel, G.E. Scuseria, M.A. Robb, J.R. Cheeseman, G. Scalmani, V. Barone, B. Mennucci, G.A. Petersson, H. Nakatsuji, M. Caricato, X. Li, H.P. Hratchian, A.F. Izmaylov, J. Bloino, G. Zheng, J.L. Sonnenberg, M. Hada, M. Ehara, K. Toyota, R. Fukuda, J. Hasegawa, M. Ishida, T. Nakajima, Y. Honda, O. Kitao, H. Nakai, T. Vreven, J.A. Montgomery, Jr., J.E. Peralta, F. Ogliaro, M. Bearpark, J.J. Heyd, E. Brothers, K.N. Kudin, V.N. Staroverov, R. Kobayashi, J. Normand, K. Raghavachari, A. Rendell, J.C. Burant, S.S. Iyengar, J. Tomasi, M. Cossi,N. Rega, J.M. Millam, M. Klene, J.E. Knox, J.B. Cross, V. Bakken, C. Adamo, J. Jaramillo, R. Gomperts, R.E. Stratmann, O. Yazyev, A.J. Austin, R. Cammi, C. Pomelli, J.W. Ochterski, R.L. Martin, K. Morokuma, V.G. Zakrzewski, G.A. Voth, P. Salvador, J.J. Dannenberg, S. Dapprich, A.D. Daniels, O. Farkas, J.B. Foresman, J.V. Ortiz, J. Cioslowski, D.J. Fox, Gaussian, Inc., Wallingford, CT, 2009.
[18] S. Chidangil, M.K. Shukla, P.C. Mishra, J. Mol. Model 4 (1998) 250–258.
[19] J.S. Murray, K. Sen, Molecular Electrostatic Potentials, Concepts and Applications, Elsevier, Amsterdam, 1996.
[20] R.I. Dennington, T. Keith, J. Millam, GaussView, Version 5.0.8, Semichem. Inc., Shawnee Mission, KS, 2008.
[21] R. Ditchfield, Mol. Phys. 27 (1974) 789–807.
[22] K. Wolinski, J.F. Hinton, P. Pulay, J. Am. Chem. Soc. 112 (1990) 8251–8260.
[23] V. Krishnakumar, G. Keresztury, T. Sundius, R. Ramasamy, J. Mol. Struct. 702 (2004) 9–21.
[24] G. Chisholm, A.R. Kennedy, S. Wilson, S.J. Teat, Acta Cryst. B56 (2000) 1046–1053.
[25] G. Chisholm, A.R. Kennedy, L. Beaton, E. Brook, Acta Cryst. C58 (2002) o645–o648.
[26] Y. Wang, S. Saebar, C.U. Pittman Jr., J. Mol. Struct. (Theochem) 281 (1993) 91–98.
[27] A.E. Reed, F. Weinhold, J. Chem. Phys. 83 (1985) 1736–1740.
[28] A.E. Reed, R.B. Weinstock, F. Weinhold, J. Chem. Phys. 83 (1985) 735–746.
[29] J.M. Seminario, Recent Developments and Applications of Modern Density Functional Theory, vol. 4, Elsevier, Amsterdam, 1996. pp. 800–806.
[30] I. Fleming, Frontier Orbitals and Organic Chemical Reactions, John Wiley and Sons, New York, 1976. pp. 5–27.
[31] I.E. Reed, F. Weinhold, J. Chem. Phys. 78 (1983) 4066–4073.
[32] K. Fukui, Science 218 (1982) 747–754.
[33] J.P. Foster, F. Weinhold, J. Am. Chem. Soc. 102 (1980) 7211–7218.
[34] V.R. Dani, Organic Spectroscopy, Tata McGraw–Hill, New Delhi, 1995.
[35] B.K. Sharma, Spectroscopy, Goel Publishing House, Meerut, 1999.

[36] Y.R. Sharma, Elementary Organic Spectroscopy, S. Chand, New Delhi, 2000.
[37] H.O. Kalinowski, S. Berger, S. Braun, Carbon-13 NMR Spectroscopy, John Wiley & Sons, Chichester, 1988.
[38] K. Pihlaja, E. Kleinpeter (Eds.), Carbon-13 Chemical Shifts in Structural and Sterochemical Analysis, VCH Publishers, Deerfield Beach, 1994.
[39] B. Osmiałowski, E. Kolehmainen, R. Gawinecki, Magn. Res. Chem. 39 (2001) 334–340.
[40] L.J. Bellamy, The Infrared Spectra of Complex Molecules, third ed., Wiley, New York, 1975.
[41] G. Varsanyi, Assignments for Vibrational Spectra of Seven Hundred Benzene Derivaties, vol. I, Adam Hilger, London, 1974.
[42] S.F. Tayyari, F. Naghavi, S. Pojhan, R.W. McClurg, R.E. Sammelson, J. Mol. Struct. 987 (2011) 241–254.
[43] J.H.S. Green, D.J. Harrison, Spectrochim. Acta 29A (1973) 1177–1188.
[44] S. Mohan, N. Puviarasan, V. Ilangovan, Arab. J. Sci. Eng. 1A (2000) 25–29.
[45] V. Arjunan, S. Mohan, S. Subramanian, B. Thimme Gowda, Spectrochim. Acta 60A (2004) 1141–1159.
[46] V. Arjunan, N. Puviarasan, S. Mohan, Spectrochim. Acta 64A (2006) 233–239.
[47] A. Altun, K. Golcuk, M. Kumru, J. Mol. Struct. (Theochem) 637 (2003) 155–169.
[48] L.J. Bellamy, The Infra-red Spectra of Complex Molecules, John Wiley and Sons Inc., New York, 1975.
[49] D.L. Vein, N.B. Colthup, W.G. Fateley, J.G. Grasselli, The Handbook of Infrared and Raman Characteristic Frequencies of Organic Molecules, Academic Press, New York, 1991.
[50] N.B. Colthup, L.H. Daly, S.E. Wiberley, Introduction to Infrared and Raman Spectroscopy, Academic Press, New York, 1990.
[51] V. Arjunan, T. Rani, C.V. Mythili, S. Mohan, Eur. J. Chem. 2 (2011) 70–76.
[52] V. Arjunan, P. Ravindran, K. Subhalakshmi, S. Mohan, Spectrochim. Acta 74A (2009) 607–616.
[53] I.F. Shishkov, L.V. Khristenko, L.V. Vilkov, S. Saamdal, Struct. Chem. 14 (2003) 51–157.
[54] V. Arjunan, S. Mohan, J. Mol. Struct. 892 (2008) 289–299.
[55] M.F. Budyka, T.S. Zyubina, A.K. Zarkadis, J. Mol. Struct. (Theochem) 594 (2002) 113–125.
[56] V. Arjunan, R. Santhanam, S. Sakiladevi, M.K. Marchewka, S. Mohan, J. Mol. Struct. 1037 (2013) 305–316.
[57] V. Arjunan, Arushma Raj, C.V. Mythili, S. Mohan, J. Mol. Struct. 1036 (2013) 326–340.